Shear behaviour of reinforced concrete beams strengthened with ultra-high performance fiber reinforced concrete (UHPFRC)

Huang, Yitao; Gu, Dawei; Mustafa, Shozab; Grünewald, Steffen; Luković, Mladena

DOI
10.1016/j.cscm.2023.e02441

Publication date
2023

Document Version
Final published version

Published in
Case Studies in Construction Materials

Citation (APA)
Huang, Y., Gu, D., Mustafa, S., Grünewald, S., & Luković, M. (2023). Shear behaviour of reinforced concrete beams strengthened with ultra-high performance fiber reinforced concrete (UHPFRC). *Case Studies in Construction Materials*, *19*, Article e02441. https://doi.org/10.1016/j.cscm.2023.e02441

Case Studies in Construction Materials 19 (2023) e02441

Contents lists available at ScienceDirect

Case Studies in Construction Materials

journal homepage: www.elsevier.com/locate/cscm

Shear behaviour of reinforced concrete beams strengthened with ultra-high performance fiber reinforced concrete (UHPFRC)

Yitao Huang [a,*], Dawei Gu [a,b], Shozab Mustafa [a], Steffen Grünewald [a,c], Mladena Luković [a]

[a] Faculty of Civil Engineering and Geosciences, Delft University of Technology, Delft, the Netherlands
[b] School of Civil Engineering, Southeast University, Nanjing, China
[c] Faculty of Engineering and Architecture, Ghent University, Ghent, Belgium

ARTICLE INFO

Keywords:
Ultra-high performance fiber reinforced concrete (UHPFRC)
Shear strengthening
Freeze-thaw
Interfacial bond strength
Finite element model
Composite member

ABSTRACT

Ultra-high performance fiber reinforced concrete (UHPFRC) is an advanced cementitious composite with high compressive strength and low permeability. Due to its excellent mechanical properties and superior durability, UHPFRC is considered promising for strengthening of the existing concrete bridges. In order to examine its strengthening efficiency for shear capacity, an experimental study is carried out on shear-deficient beams without stirrups. Strengthening method comprising precast UHPFRC laminates being glued with epoxy resin on two lateral sides of the reinforced concrete beams, is examined. To investigate the robustness of the system under severe exposure conditions, some beams are subjected to freeze-thaw (FT) cycles. Beams are tested to failure under three-point bending configuration. Test results show that for epoxy resin bonding, UHPFRC shear strengthening is a promising method to increase the load and deformational capacity, and to limit the crack openings. The load capacity is doubled, and the deformational capacity is increased by around 60%. After exposure to 30 FT cycles, the strengthening efficiency and fracture behaviour of UHPFRC composite beams seem not to be affected. It seems that the interfacial bond strength is sufficient to prevent premature debonding between UHPFRC and NC, which under combined action of environmental exposure (e.g. FT) and mechanical loading might become a challenge. Finally, a finite element model is developed to predict and understand the shear behaviour of the reference and strengthened beams. In general numerical results show good agreement with the experimental results in terms of failure pattern and peak load prediction once the perfect bond model is used for the interface between UHPFRC and NC. In order to better understand the role of governing parameters on the shear capacity of the composite member, parametric studies are conducted focusing on the role of varying UHPFRC softening behaviour and UHPFRC-concrete interface properties.

1. Introduction

Ultra-high performance fiber reinforced concrete (UHPFRC) is characterized as an innovative cementitious material with very high strength (also in tension but primarily in compression) and superior durability [1] due to the high packing density accompanied by the

* Corresponding author.
E-mail address: Y.Huang-6@tudelft.nl (Y. Huang).

https://doi.org/10.1016/j.cscm.2023.e02441
Received 21 June 2023; Received in revised form 9 August 2023; Accepted 29 August 2023
Available online 1 September 2023

addition of steel fibers. Despite the better performance compared to conventionally used normal concrete (NC), UHPFRC has higher costs and a larger environmental impact when compared per unit volume, limiting its wide use [2]. However, considering the whole life cycle analysis and entire (including indirect) project costs, some applications of UHPFRC largely overweigh the benefits of using NC [3–5], one of them being strengthening of existing concrete structures [6–12].

In view of the excellent properties of fiber reinforced concrete such as engineered cementitious composite (ECC) and UHPFRC, numerous studies have been devoted to investigating performance of concrete structures repaired with these novel cementitious materials [13–16]. For UHPFRC strengthening application, the majority of research to date has focused on flexural performances of reinforced concrete (RC) beams retrofitted by UHPFRC, which is summarized in [17]. This research has clarified that UHPFRC can significantly increase the flexural resistance of RC beams, showing its potential as a strengthening material in flexure. However, as illustrated in [18], there are still knowledge gaps with respect to shear performance of RC beams strengthened with UHPFRC, which is critical, especially considering its brittle nature. Although the existing studies prove that UHPC beams show significantly higher shear strength and ductility compared to RC beams due to the existence of steel fibers [19–21], only few studies are devoted to the analysis of shear response of UHPFRC-RC composite members [8,12,22–26]. In order to investigate the mechanical efficiency of UHPFRC, Hussein et al. [25] compared the shear resistance of reinforced composite beams made of UHPFRC and NC (UHPFRC-NC), and of UHPFRC and High Strength Concrete (UHPFRC-HSC), to their reference NC and HSC beams. It was found that UHPFRC greatly enhanced the shear capacity of all composite members both containing NC and HSC. In addition, the influence of strengthening configurations on the shear behaviour of reinforced concrete members with UHPFRC has been studied in several works [12,22,26]. For example, the effectiveness of two strengthening schemes: (a) one lateral side strengthening and (b) two lateral sides strengthening using epoxy were experimentally and numerically investigated by Sakr et al. [12]. Results show that two lateral sides strengthening scheme leads to higher shear loads compared to one lateral side strengthening. Still, knowledge is lacking on how various parameters such as bond methods, exposure conditions, reinforcement in UHPFRC and material properties of UHPFRC play a role in the shear performance of such composite structures.

In order to guarantee the composite action and shear strengthening efficiency of UHPFRC, the bonding behaviour between embedded reinforcement and UHPFRC [27,28], and between UHPFRC and concrete substrates [18,29,30] should be studied. Since the UHPFRC does not have embedded reinforcement in this study, the focus is put on the bond between UHPFRC and existing concrete as the delamination at the interface between the two concretes should be avoided [12]. Typically, UHPFRC can either be cast in-situ or applied as precast laminates. For cast in-situ UHPFRC application, the shrinkage-induced stress is a noticeable problem especially considering that UHPFRC has a larger shrinkage (especially autogenous shrinkage) than NC [31,32]. While according to parametric studies in FE modelling [33], it is found that shrinkage will not greatly affect the response of UHPFRC-reinforced concrete structures. However, a more comprehensive experimental study conducted by Zhu et al. [31] shows that shrinkage-induced stress cannot be simply ignored since different curing conditions will directly affect the shrinkage results and the safety of the bond is hard to determine due to unclear bond parameters between UHPFRC and NC substrate. For precast UHPFRC laminates, two main bonding techniques are used: bonding with epoxy resin and mechanical anchorage. The use of mechanical bolts will reduce the strengthening area of UHPFRC, damage the concrete substrate and lead to the stress concentration around the bolts [34,35]. Epoxy resin is preferable to connect the concrete and precast UHPFRC compared to mechanical anchorage, though it is more sensitive to thermal and hygral changes [12]. Therefore, one of the goal in this study is to examine the shear strengthening efficiency of 10 mm thick epoxy-bonded UHPFRC precast lamellas. Besides resistance to mechanical loads, the damage in multi-material composite might initiate due to restrained deformations caused by temperature and moisture gradients, especially under harsh environmental conditions. This might affect the long-term behaviour of the bond between the UHPFRC and the existing concrete, and durability of strengthened structures. So far, no research has been carried out on combined actions of imposed loads and imposed deformations, which might cause the progressive degradation of the hybrid structure and the interface between UHPFRC and NC bond. Therefore, the aim of this study is also to evaluate the effect of freeze-thaw conditions on the composite member and its effect on residual load-carrying capacity. Besides structural tests, also material tests were executed to determine the material properties of UHPFRC, including the compressive and tensile strengths, the elastic modulus, and shrinkage. The fracture behaviour of RC reference beams and UHPFRC-RC composite beams were critically assessed. Finally, based on the experimental results, numerical model using commercially available ATENA finite element software was built to predict and evaluate the role of governing parameters on the shear behaviour of RC beams strengthened with UHPFRC.

2. Material characteristics

2.1. Proportion of NC and UHPFRC

In this study, concrete strength class C20/25 (w/c ratio 0.60) is used in the fabrication of reinforced concrete beams and the purpose of using weak concrete is to simulate the concrete deterioration in existing bridges. The concrete consists of cement 42.5 N, aggregates with maximum aggregate size of 16 mm, water and superplasticizer (Table 1). For the UHPFRC mixture, cement 52.5 R,

Table 1
Mix design details (in kg/m^3).

Mixture	Cement	Silica fume	Sand	Gravel	Water	Superplasticizer (Master Glenium 51)	Fiber
Concrete	260	-	847	1123	156	0.26	-
UHPFRC	850.5	100	1113.2	-	177	42	200

silica fume, and fine sands having a maximum aggregate size of 1 mm are used. First, the water and superplasticizer are mixed with dry particles, subsequently followed by addition of 2.5% (by volume) straight steel fibers with a diameter of 0.16 mm and a length of 6 mm (aspect ratio equals 37.5).

2.2. Mechanical and volume stability tests on NC and UHPFRC

The compressive strength of the NC and UHPFRC is determined based on NEN-EN 12390 [36], using cubical specimens with dimensions of 100 mm and 40 mm respectively. In order to measure the elastic modulus of NC and UHPFRC, two prisms ($100 \times 100 \times 400$ mm^3) are tested by a Tonibank hydraulic Instron. Linear variable differential transducers (LVDTs) are vertically attached on the four sides of specimens to measure the deformation over a gauge length of 135 mm under the compressive load. The loading and unloading rates are 1 kN/s and each sample goes through three cycles with the stress ranging from 0.5 MPa until a compressive stress corresponding to 30% of its compressive strength.

Splitting tensile test is conducted to get the tensile strength of concrete, while for UHPFRC, dog-bone specimens (recommended by JSCE [37]) are cast and direct tension test is employed to get its tensile response (Fig. 1). Note that the thickness of the dog-bone specimen (13 mm) is larger than that of the applied laminates (10 mm) for strengthening. Since the thinner specimens generally have better and preferential fiber orientation, resulting in better tensile properties of UHPFRC [38], it is assumed that the measured tensile response will be on conservative side. The test is conducted under the constant loading rate of 0.003 mm/s and the deformation of the specimens over a gauge length of 80 mm are recorded by two LVDTs attached on the specimen.

Although shrinkage-induced stresses are less relevant for the current study (lamellas were bonded to concrete at a later age, i.e. of more than 28 days), if the curing duration of UHPFRC lamellas is shortened or UHPFRC is cast in-situ, the role of shrinkage induced stresses should be considered [39–41]. Therefore, as shown in Fig. 2, both the autogenous shrinkage and total shrinkage are measured for UHPFRC from the age of 1 day. Six UHPFRC specimens with the dimension of $40 \times 40 \times 160$ mm^3 are cast. At the age of one day, specimens are demoulded. Autogenous shrinkage measurement is performed on three specimens which are wrapped with aluminum foil and sealed with tape to avoid moisture loss. Other three samples, on which drying shrinkage measurement is performed, are left unsealed. All specimens are placed in a room with a constant temperature of 20 ± 2 ºC and a relative humidity of 50 ± 5%. The free deformation measurement is performed by using a comparator (accuracy of 0.001 mm) in accordance with requirements of the ASTM C157 [42].

2.3. Freeze-thaw tests on NC and UHPFRC

For freeze-thaw test, 30 freeze thaw cycles are chosen. As estimated in [43], the average number of FT cycles in the Netherlands is around 30 cycles per year or per two years dependent on the employed criteria to define a FT cycle. In this study, the experiment is designed to investigate the performance of UHPFRC strengthened concrete structures during the initial service period (first year or first two years), as it might be the most susceptible period when freeze thaw action might damage the material mechanical properties [44] and the bond between strengthening material and the existing concrete [45–47]. To investigate the influence of freeze-thaw (FT) cycles on the material properties of NC and UHPFRC at an age of more than 28 days, their compressive strength is measured after 30 FT cycles. Freezing and thawing process is done in dry condition with a relative humidity ranging from 50% to 70%, in order to represent realistic climate conditions for concrete bridges. One FT cycle lasts for about 24 h at the temperature ranging from − 20–20 ℃ and it consists of two stages, as shown in Fig. 3. In stage I, the specimens are placed at sustained room temperature (20 ℃) for 8 h. Stage II consists of a rapid cooling process in freezing chamber, where the specimens are exposed to a constant temperature at − 20 ℃ for 16 h. After completion of the predefined 30 FT cycles, compressive strength of concrete and UHPFRC cubes are measured.

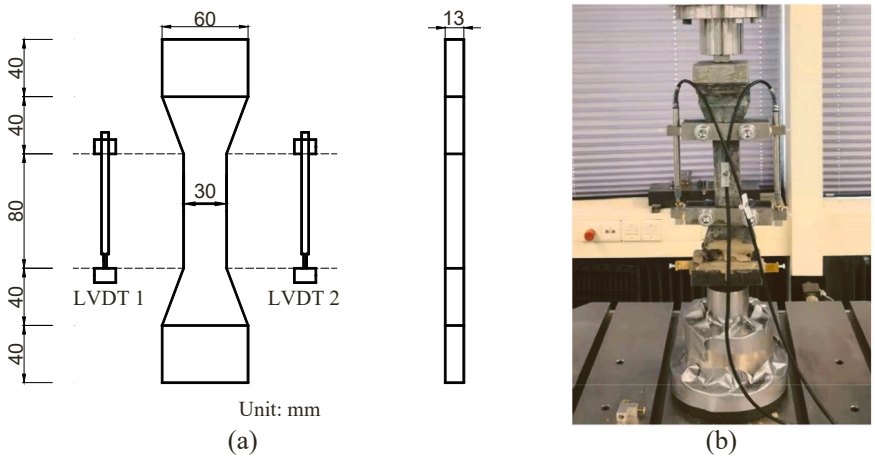

Fig. 1. Direct tensile tests (a) geometry and (b) experimental setup.

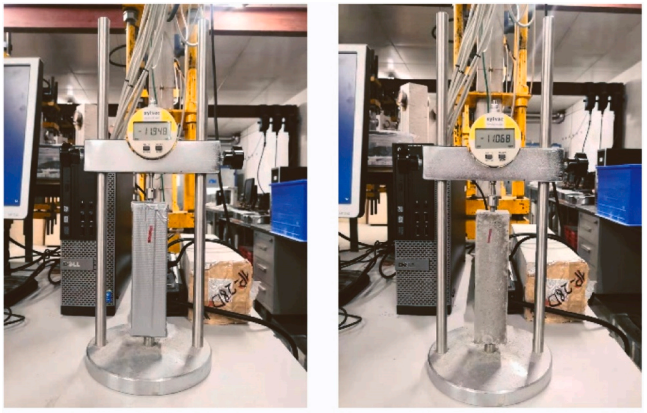

Fig. 2. Testing set-up for autogenous and total shrinkage measurement on UHPFRC: (a) autogenous shrinkage measurement; (b) total shrinkage measurement.

2.4. Material properties of NC and UHPFRC

The stress-displacement relation and cracking pattern of UHPFRC specimens tested under direct tension are presented in Fig. 4. It is observed that the deformation is localized in a single crack within gauge length and tensile capacity varies considerably among different tested specimens (especially specimen 2), which aligns with prior studies on UHPFRC [33,48,49]. The large variation in the tensile response of the dog-bones is primarily governed by the distribution and orientation of fibers. The material test results, including compressive strength (with and without exposure to freeze-thaw cycles), tensile strength (splitting tensile strengthf_{sp} for NC, first cracking f_{ct} and post-crack tensile strength f_{pt} for UHPFRC) and E-modulus, at an age when structural tests were conducted are listed in Table 2. The average compressive strength, first cracking f_{ct} and post-crack tensile strength f_{pt} for UHPFRC) are 122.4 MPa, 6.9 MPa, 9.2 MPa respectively, which meets the minimum requirement for structural application with UHPFRC in terms of its mechanical properties [50]. Moreover, the freeze-thaw cycles do not significantly affect the compressive strength of UHPFRC and NC.

Fig. 5 presents the average autogenous shrinkage and total shrinkage (including autogenous and drying) for UHPFRC from the age of one day. Based on more than 90 days' of shrinkage measurements, it is observed that both the autogenous shrinkage and total shrinkage strain reach a plateau at around 50 days after casting. The autogenous shrinkage nearly accounts for two-thirds of the total shrinkage, which agrees with the findings in [51]. Under the same curing conditions, the total shrinkage of UHPFRC is nearly the same as that of conventional concrete with a compressive strength lower than 50 MPa for which the total shrinkage is in range of 400–600 με [52]. However, for UHPFRC, a significant part of autogenous shrinkage occurs at a very early age (within the first 24 h) [53], which is not measured in this test. Therefore, the measured value is estimated to be only about half of the total shrinkage strain which can form

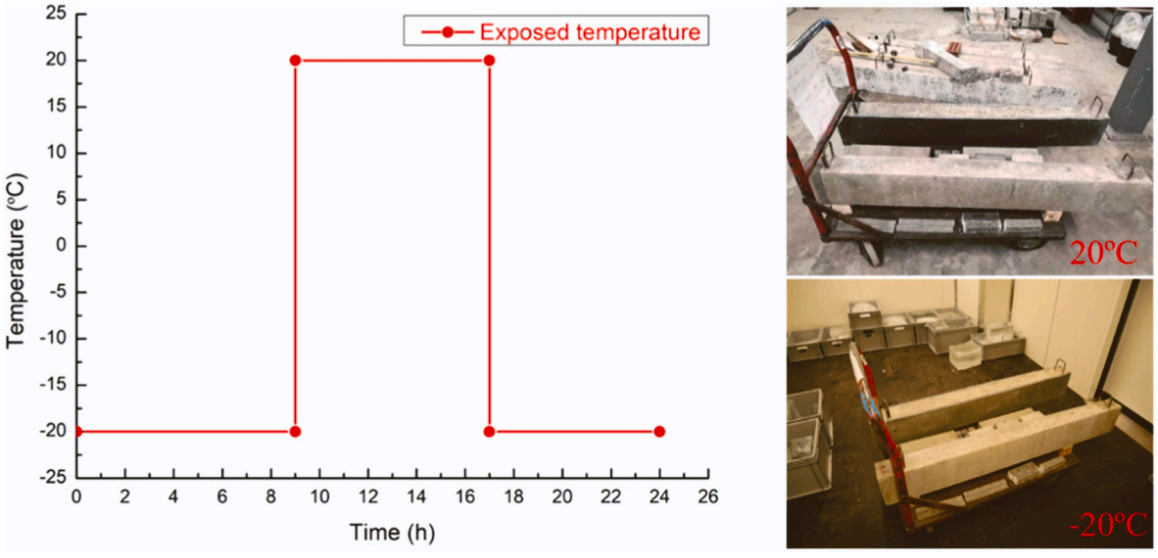

Fig. 3. Freeze-thaw protocol on specimens.

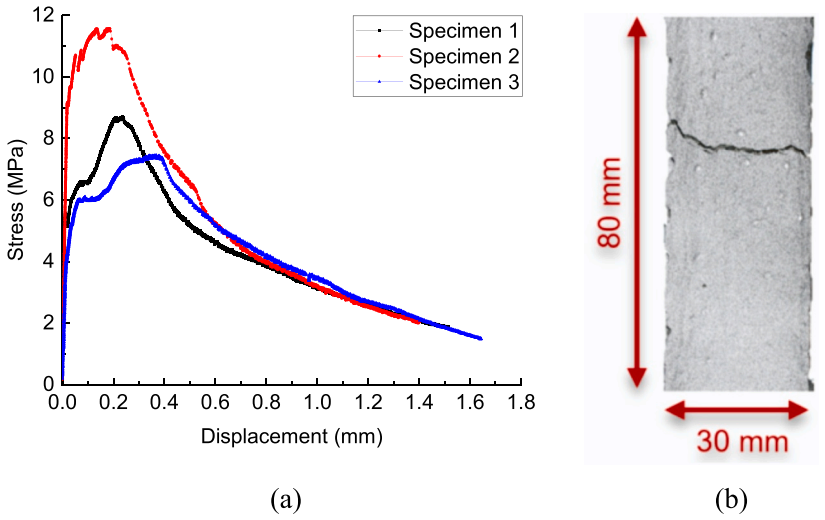

Fig. 4. Tensile properties of UHPFRC: (a) Stress-displacement behaviour of UHPFRC, note that the LVDT displacement is obtained over the 80 mm measurement length; (b) Cracking pattern.

Table 2
Mechanical properties (average ± standard deviation) of cement-based materials.

Mixture	Compressive strength (MPa)		Tensile strength (MPa)			Elastic modulus (GPa)
	0 FT cycle	30 FT cycles	f_{sp}	f_{ct}	f_{pt}	
Concrete	35.2 ± 1.5	33.8 ± 5.3	3.4 ± 0.7	-	-	35.3 ± 1.5
UHPFRC	122.4 ± 5.1	125.4 ± 8.7	-	6.9 ± 2.0	9.2 ± 2.1	45.2 ± 1.1

from the onset of autogenous shrinkage (commonly defined as zero-time [54]) and can reach approximately 1000 με for comparable UHPFRC mixtures with small aggregate size [55].

3. Structural tests

3.1. Specimen setup for reinforced concrete (RC) and strengthened beams

Four reinforced concrete (RC) specimens were fabricated. The beams contained two 16 mm diameter rebars at the bottom (tensile zone). No stirrup in the region of the effective span was used to imitate the concrete deck without shear reinforcement built before

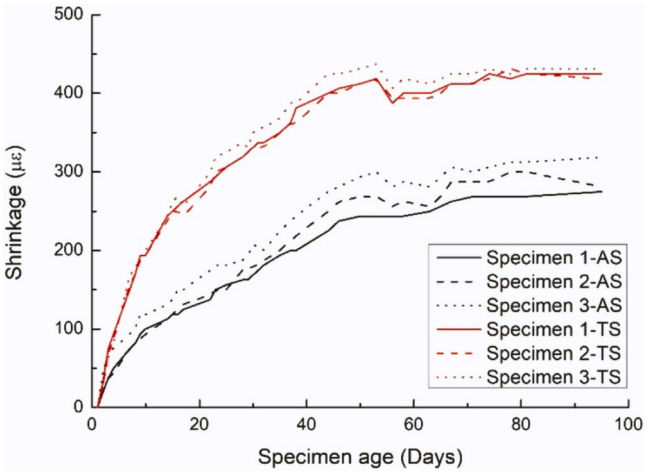

Fig. 5. Autogenous and total shrinkage curves for UHPFRC measured from the age of one day (AS and TS denote the autogenous and total shrinkage respectively).

1970 s in the Netherlands (two stirrups were placed outside of the supports to lift the beams). The geometry of the beams and the reinforcement details are presented in Fig. 6.

Two of these beams are used as reference beams (RB) exposed to 30 FT cycles according to the freeze-thaw protocol described in Section 2.3, and the two other beams are strengthened with 10 mm thickness UHPFRC on both lateral sides (Fig. 7). In order to reduce the adverse effect of restrained shrinkage, UHPFRC laminates are precast and cured for more than 28 days to eliminate major part of shrinkage at the initial stage (shown in Fig. 5), before being bonded to concrete. Epoxy-bonded technique is used and consisted of bonding two prefabricated UHPFRC laminates to the concrete beams using 1 mm thick Sikadur®− 30, a two-component epoxy adhesive. Sikadur®− 30 is a commercial epoxy adhesive which is commonly used for strengthening application of concrete structures, and it consists of a resin (part A) and a hardener (part B) with a mixing A/B ratio of 3. Both components (A and B) are mixed in a bucket using a power drill for at least 3 min in order to achieve the homogeneity of the epoxy resin. The main properties of Sikadur®− 30 are listed in Table 3. Prior to application of epoxy resin, the interface is treated with air jet to blow away the dust and is subsequently cleaned with ethanol. The surface of RC beams is smooth prior to application of UHPFRC. After applying the epoxy, the clamps are used to keep tight the UHPFRC laminate and concrete (Fig. 8). Among the two strengthened beams, one of them is exposed to 30 FT cycles. Table 4 summarizes the beam details.

3.2. Test setup

All beam specimens, with or without exposure to FT cycles, are tested under three-point bending. The test is performed with a displacement-controlled jack loading the beams at a rate of 0.01 mm/sec. Fig. 9 shows a schematic of the test setup. In order to simulate the realistic boundary conditions in strengthening application, the applied load and support plates are only placed on the NC part in the strengthened beam. For reference beams, LVDTs with an accuracy of 0.001 mm are used to measure displacement at midspan and strain distribution along the height of the beams. For strengthened beams, apart from mid-span deflection, measured on concrete part, and strain measurement at the surface of UHPFRC, LVDTs are used to measure the interface slip and opening near the loading point, as shown in Fig. 9(b). Based on the findings in [33,56], the maximum slip will be observed in mid-span of the beams strengthened with UHPFRC. Therefore, in order to detect the interface behaviour and possible delamination of the critical zone for strengthened beams, four locations near the loading point are selected. LVDT 3, 6, 8 and 10 are used to detect the interface opening, and LVDT 2, 4, 7 and 9 are used to detect the interface slip between UHPFRC and NC at those locations.

In addition to the LVDT measurement system, Digital Image Correlation (DIC) is used from the other lateral side of the beams. DIC is a non-contact image-based measurements technique, used to capture the strain field and fracture development in the beams during the loading process. In the DIC measurement system, 51 Megapixel camera with 8688 by 5792 pixels is used to capture the images with a resolution of 0.125 mm/pixel, and GOM Correlate software [57] is used for the analysis. A subset size of 19 pixels and a step size of 16 pixels are chosen for the correlation. Before the DIC analysis, the noise level is evaluated and the DIC results reported in this study have a relative deformation accuracy of 0.008 mm and a major strain accuracy of 0.075%. The schematic of the DIC setup is shown in

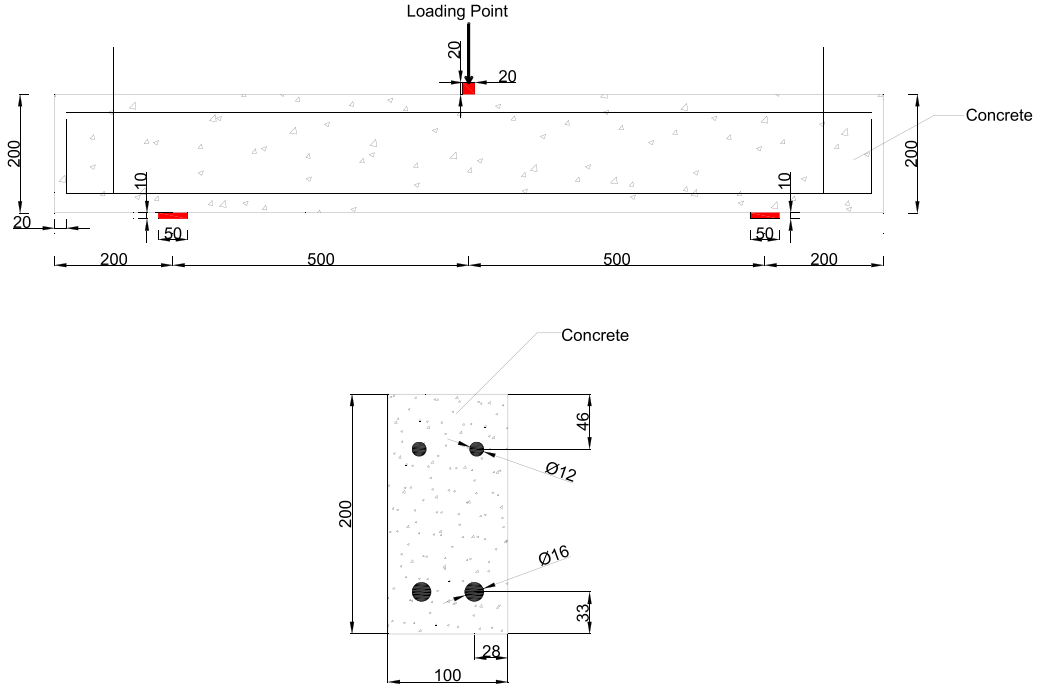

Fig. 6. Geometry of reference beam (unit: mm).

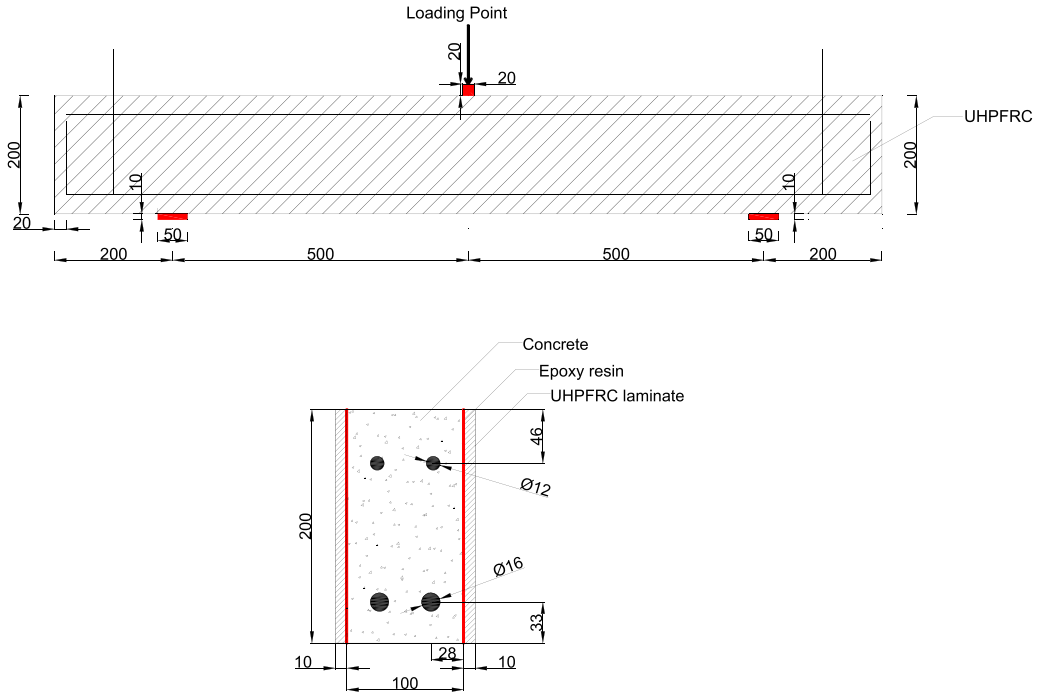

Fig. 7. Geometry of strengthened beam (unit: mm).

Table 3
The main properties of Sikadur®– 30.

Mechanical properties	-
Compressive strength (After 1 day and cured under a temperature between 10 and 35 °C)	55–90 MPa
Tensile strength (After 1 day and cured under a temperature between 15 and 35 °C)	20–26 MPa
Tensile bond strength (to concrete) after 7 days and cured under 23 °C	> 4 MPa
Shear strength (After 1 day and cured under a temperature between 15 and 35 °C)	4–17 MPa
E-modulus in compression cured under 23 °C	9.6 GPa
E-modulus in tension cured under 23 °C	11.2 GPa
Shrinkage	0.04%
Coefficient of thermal expansion	2.5×10^{-5} /°C

Fig. 10.

4. Test results

The strengthening effect of UHPFRC and damage induced by FT cycles are analyzed by comparing the load-deflection and fracture pattern between the reference beams and strengthened beams. In addition, the cracking process and shear crack displacement are evaluated. Finally, the interface properties between UHPFRC and NC with/ without FT cycles are examined.

4.1. Shear resistance and fracture pattern of the tested beams

The shear load-displacement relationship and schematic view of energy absorption for all tested beams are shown in Fig. 11. It can be observed that the application of 10 mm epoxy-bonded UHPFRC precast plates on lateral sides of the reference beam (ST-EB) significantly increases the loading, deformational, and energy absorption capacity. In addition, freeze-thaw cycles do not cause any significant damage in both reference (RB-30) and strengthened (ST-EB-30) beams, which is in line with the concrete compressive strength measurements. Table 5 presents the summary of the test results and the energy absorption, which is defined as the area under the load-deflection curve until the peak load (shown in Fig. 11 (b)). For specimens without FT cycles, due to the growth of dominant shear crack, both reference and strengthened beams show brittle failure when the load reaches the maximum bearing capacity of 59.8 kN and 126.7 kN, respectively (Fig. 11). The addition of two 10 mm prefabricated UHPFRC laminate improve the load-bearing capacity by 112%. This is higher than the shear strength gain that would be obtained by using laminates made of higher strength concrete (around 3 and 4 times higher tensile and compressive strength, respectively), which can be predicted by Eurocode equation [58]. Therefore, the shear strength gain also comes from the crack bridging of fibers [20,59]. The deflection at the maximum load for

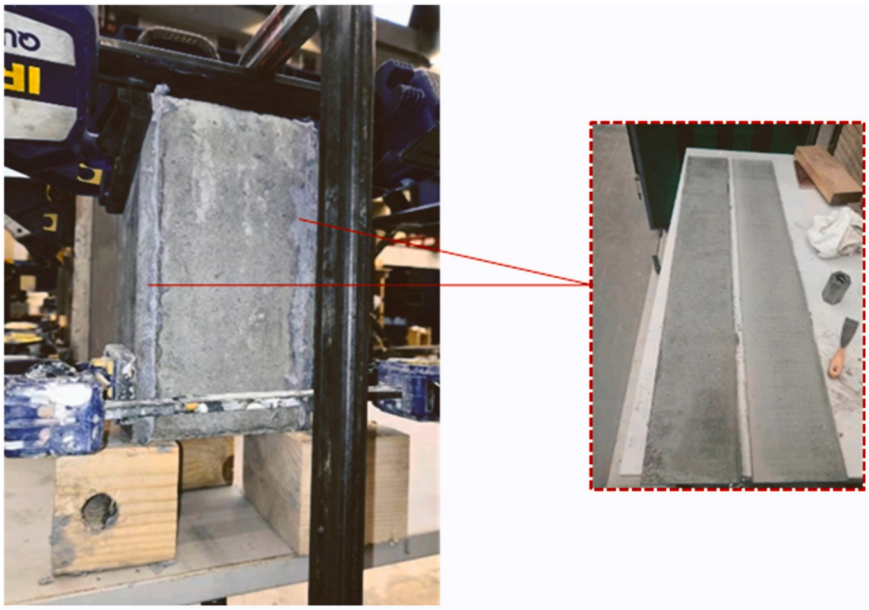

Fig. 8. Bonding precast UHPFRC laminate using epoxy resin.

Table 4
Test beam details.

Beam ID	Dimension $b \times h \times L(mm^3)$	Bonding techniques	Freeze-thaw cycles
RB	100 × 200 × 1400	-	0
ST-EB	120 × 200 × 1400	Epoxy-bonded	0
RB-30	100 × 200 × 1400	-	30
ST-EB-30	120 × 200 × 1400	Epoxy-bonded	30

RB and ST beams is found to be 2.5 mm and 3.9 mm respectively, which shows 57% deflection improvement for ST beam. In terms of stiffness, the application of UHPFRC laminates only slightly increase the initial stiffness of the beam. As load increases, the stiffness of reference beam quickly reduces compared to strengthened beam due to the earlier initiation and propagation of cracks. After experiencing 30 FT cycles, RB-30 and ST-EB-30 do not show any significant change in the shear resistance when compared to the unexposed beams (4.5% for RB-30 and 5.5% for ST-EB-30). Compared to RB-30, the deflection of the RB beam is larger due to a strut-and-tie mechanism which is activated after the formation of the dominant shear crack, which is caused by the random crack pattern. Therefore, RB beam exhibited 1.7 and 2.2 times higher deflection and energy absorption, respectively, compared to RB-30. Both ST-EB-30 and ST-EB show nearly the same initial stiffness (Fig. 11 (a)), Still, ST-EB-30 shows stiffness degradation at a lower load, and finally exhibited a slightly lower peak load compared to ST-EB. These differences are small and can be a result of the scatter in material properties, as presented in Table 2. The strengthened beams have around three times higher energy absorption than that of the reference beams.

The reference beam (RB) did not fail immediately after forming the dominant shear crack (Fig. 11). There is load transfer mechanism activated by the anchorage effect from the end of longitudinal reinforcement, which bonds the split beam and enables it to continue to resist the applied load. Fig. 15 presents the failure process of all tested beams obtained by analyzing principal strain by DIC. As shown in Fig. 12, in the RB beam, shear crack which dominates the failure of beam initiates at a load of about 42 kN. When the load is increased to 48 kN, the dominant shear crack is widened and becomes visible. At peak load (58 kN) prior to the shear failure of the RB beam, shear crack grows close to the support and loading point. After the peak load, due to the compressive failure of concrete near the loading point, the beam fails and the test is terminated. For ST-EB beam, one flexural crack develops into a critical shear crack at 100 kN. As the load increases (116 kN), the shear crack further forms along the diagonal direction to the loading point. At peak load (126 kN), concrete in the compressive zone starts to crush because the diagonal crack has grown through the whole shear plane, which makes the applied load to drop suddenly. Without obvious damage happening in specimens under freeze-thaw condition, the crack development of RB-30 and ST-EB-30 is similar to that of RB and ST-EB respectively. Fig. 13 represents the crack patterns at failure of the RB and ST-EB beams, including those exposed to FT cycles. As expected, all the tested beams failed in shear.

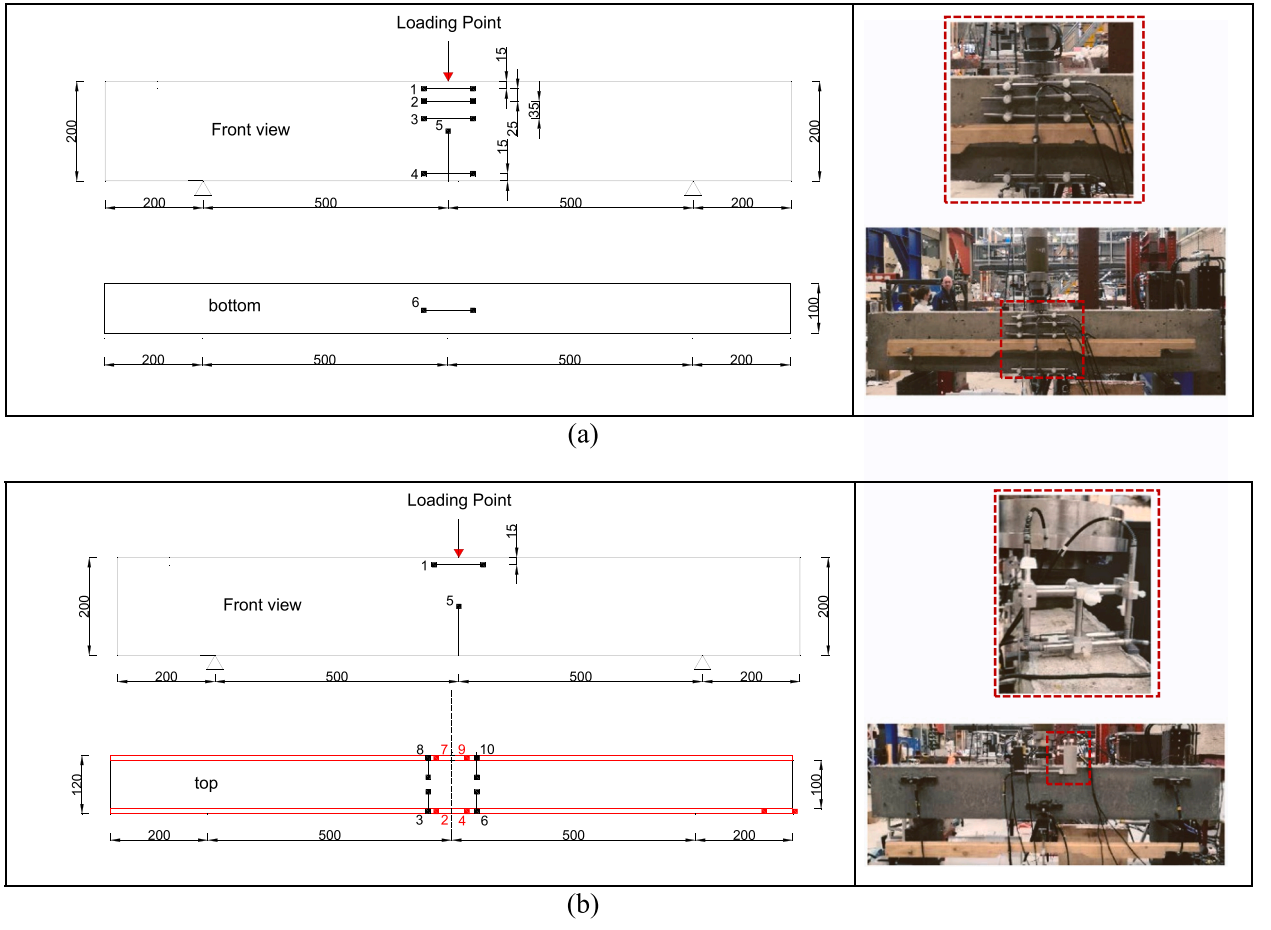

Fig. 9. Schematic of the test setup and LVDT arrangement: (a) LVDT arrangement for reference beam; (b) LVDT arrangement for hybrid beam (Unit: mm).

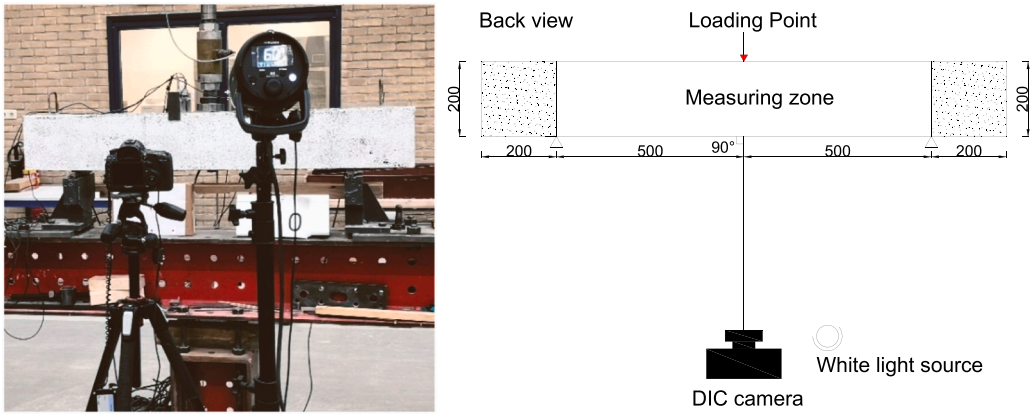

Fig. 10. Schematic of the DIC setup.

4.2. Shear crack displacement

Shear resistance of concrete beams originates partly from the friction at the cracked surface and is proportional to the principal normal stress at the shear plane [60]. Upon exceeding the shear strength, shear failure will happen and is recognized as the separation of the crack surfaces with reduction of the load. Crack slip and crack opening are coupled during the separation process. With the addition of UHPFRC, steel fibers increase the stress transfer ability in cracked concrete, which restrains the growth of crack width and potentially increase the capacity and ductility of concrete structures. In order to investigate the role of steel fibers, shear displacement including crack slip and crack opening of the critical shear crack are analyzed.

By using DIC, a 2-dimensional displacement field is generated at different load levels. From the two-dimensional surface displacement field, two reference points at the left- and right-hand side of the critical shear crack are selected and the crack opening and sliding are extracted. As shown in Fig. 14 (a), due to the global rotation of the specimen, the displacement AA' parallel to the crack path will lead to a significant error when quantifying crack slip measurement. Therefore, a 4-point reference system is used to eliminate the effect of rigid body rotation (Fig. 14 (b)).

Based on Fig. 14 (b), the reference points are grouped into kinematic points (A and B) and rotation points (C and D). After certain applied load, the specimen deforms and global rotation occurs, kinematic points (A and B) and rotation points (C and D) are turned into new position, which are named A' and B', C' and D'. The rigid rotation angle $\theta$is defined as the angle change:

$$\theta = \frac{1}{2}\left(\theta_1 + \theta_2\right) = \frac{1}{2}\left(\arccos\frac{\overrightarrow{AC}\cdot\overrightarrow{A'C'}}{\left|\overrightarrow{AC}\right|\cdot\left|\overrightarrow{A'C'}\right|} + \arccos\frac{\overrightarrow{BD}\cdot\overrightarrow{B'D'}}{\left|\overrightarrow{BD}\right|\cdot\left|\overrightarrow{B'D'}\right|}\right) \tag{1}$$

Then the angle change due to applied load is:

$$\alpha = \arccos\frac{\overrightarrow{AB}\cdot\overrightarrow{A'B'}}{\left|\overrightarrow{AB}\right|\cdot\left|\overrightarrow{A'B'}\right|} - \theta \tag{2}$$

Finally, the crack slip displacements are obtained using the following expressions:

$$Crackopening = \left|\overrightarrow{A'B'}\right|\cos\alpha - \left|\overrightarrow{AB}\right| \tag{3}$$

$$Cracksliding = \left|\overrightarrow{A'B'}\right|\sin\alpha \tag{4}$$

With the aforementioned proposed equation, crack slip and opening could be extracted. For each specimen, four different groups of points along the shear crack propagation path are selected, as shown in Fig. 15. Measured crack opening and sliding from four groups of points along the major crack are shown in Fig. 16. Fig. 17 shows a comparison of average crack opening and sliding between the major shear crack of every test beam to reflect the full response of the beam.

From DIC analysis of RB and RB-30 beams (Figs. 16 and 17), it is observed that the crack opening happens earlier than the sliding along the shear crack plane. When the load is close to reaching the peak, the crack slip increases rapidly and shear crack opens fast (Fig. 16). Compared to RB beam (Fig. 16 a), RB-30 beam (Fig. 16 c) shows a more brittle failure as it loses the shear resistance at lower maximum deflection and crack displacement. Close to the peak load, the critical shear crack occurs and the crack displacement rapidly increases, followed by the sudden shear failure. ST-EB and ST-EB-30 beams exhibit similar response as that of RB beams. However, crack opening and sliding significantly increases when the load level is around 90% of peak load, indicating that there is still a remaining bearing capacity before the final shear failure happens. Steel fibers inside the UHPFRC enable a more ductile response of the

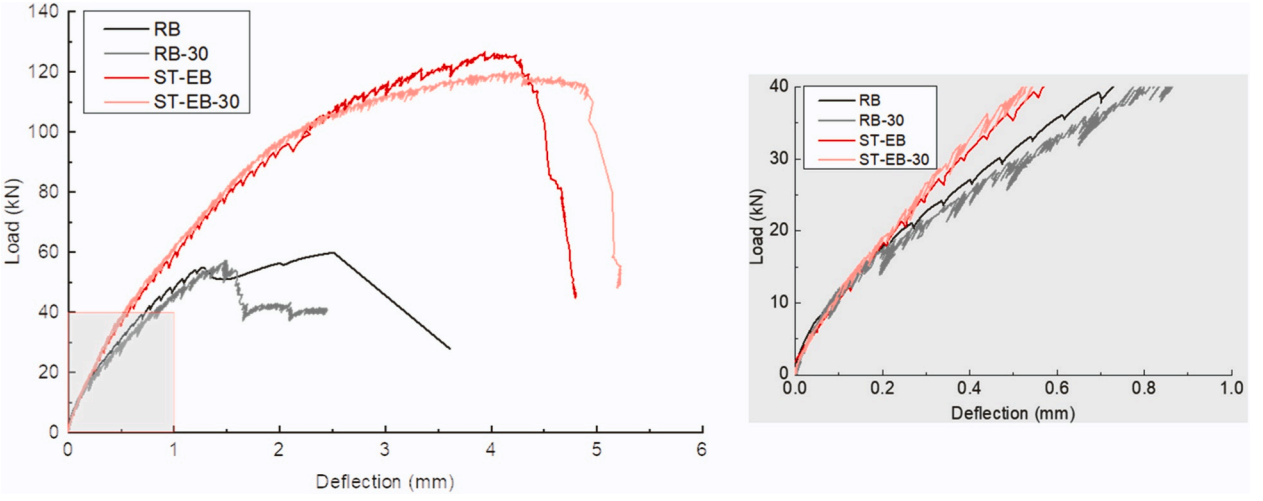

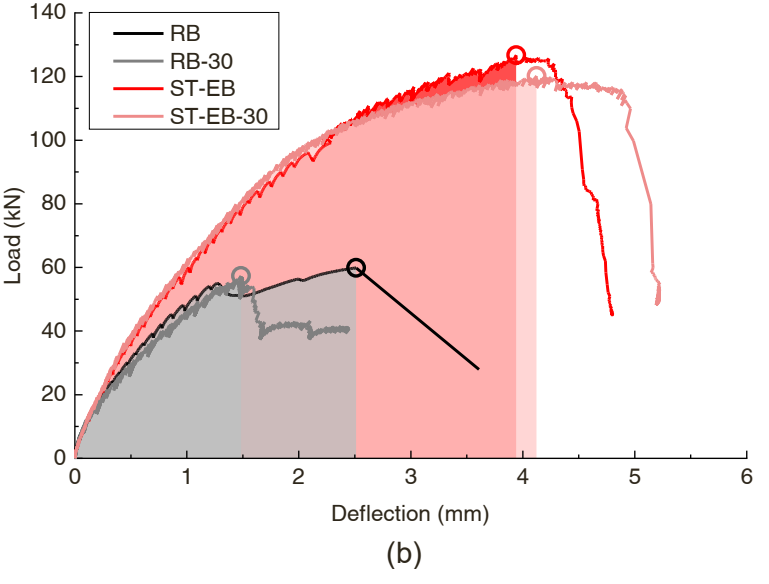

Fig. 11. Load-displacement relationship of RB and ST beams and schematic view of energy absorption: (a) load-displacement curve for RB and ST beams together with zoomed view of initial response; (b) schematic view of energy absorption for each specimen.

Table 5
Results in terms of load, deflection, energy absorption and failure mode.

Beam specimen	Peak load (kN)	Deflection at peak load Δ_{exp}	Energy absorption (kN·mm)	Capacity increase due to strengthening $(\frac{P_{ST-EB-i}-P_{RB-i}}{P_{RB-i}})$ (%)	Capacity decrease after FT $(\frac{P_j-P_{j-30}}{P_j})$ (%)	Failure pattern
RB	59.8	2.51	112.5	-	-	Shear failure
ST-EB	126.7	3.94	331.0	112	-	Shear failure
RB-30	57.3	1.48	52.2	-	4.5	Shear failure
ST-EB-30	119.7	4.19	351.3	109	5.5	Shear failure

Note: i represents the number of FT cycles, j denotes RB without or with the application of UHPFRC.

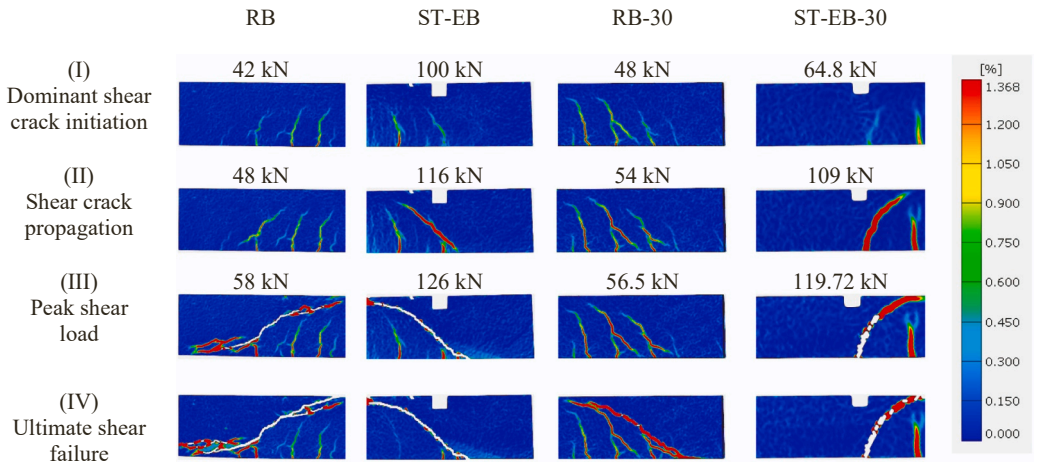

Fig. 12. Crack propagation at different load stages.

strengthened beam. Owing to the good FT resistance of UHPFRC, ST-EB and ST-EB-30 behave in a similar way in terms of crack displacement. Moreover, as shown in Fig. 17 (a), with the addition of steel fibers, the crack opening and sliding significantly reduce under the same deformation level compared to RB beams. Finally, a larger maximum crack slip and opening could be achieved before the peak load. This demonstrates that the steel fibers restrain the crack development, enable more warning before failure and finally improve the shear resistance. Interesting to notice is that it seems that there is a unique relation between the crack sliding and crack opening for all the beams (Fig. 17 (b)), with crack opening being governing at the lower loads and crack sliding becoming dominant at higher load levels.

4.3. Interface property

Though stress induced by restrained shrinkage (generally occurs for cast in-situ bonding technique) is largely reduced for hardened precast UHPFRC laminates bonded with epoxy resin, the interface behaviour will still govern the performance and failure mode of strengthened beam. Based on the findings in [33,56], for two-sided and three-sided strengthening schemes, the maximum slip and possible detachment will occur in the mid-span where the load is applied. Therefore, in order to capture the interface behaviour in the most critical zone, as illustrated in Fig. 9(b), LVDTs to measure the interface opening and sliding are used. As the LVDT could not be placed exactly at the loading point, they are attached closely to the loading point where the maximum deflection is reached (at a distance of around 15 cm from the loading point).

Load versus interface slip and opening curves are plotted for ST-EB and ST-EB-FT beams, as shown in Fig. 18. Note that since the accuracy of LVDT (1 μm) has the same order of magnitude as interface displacement, there is a lot of noise during the measuring process. From Fig. 18, though four LVDTs are placed at a same distance from the center loading point and the configuration of beam is symmetrical, the slip at different measurement points differs. This might be explained by the asymmetrical cracks induced by the applied load. From the trend of load versus interface slip and opening, it is found that the interface slip and opening increase with the applied load until the load level of around 100 kN. When the applied load exceeds 100 kN and major shear crack occurs, the interface slip and opening show reduction. This might be due to the stress redistribution once the major shear crack occurs. However, further studies are needed to validate and quantify the interface behaviour.

The maximum slip and opening during the whole loading process are less than 7 μm and 16 μm, respectively. As stated in *fib* Bulletin 43 [61], the maximum interface slippage allowance is 0.2 mm under the serviceability limit state and 2.0 mm under the ultimate limit state. The small slip and opening prove that no interface delamination is observed and the interface still keeps intact

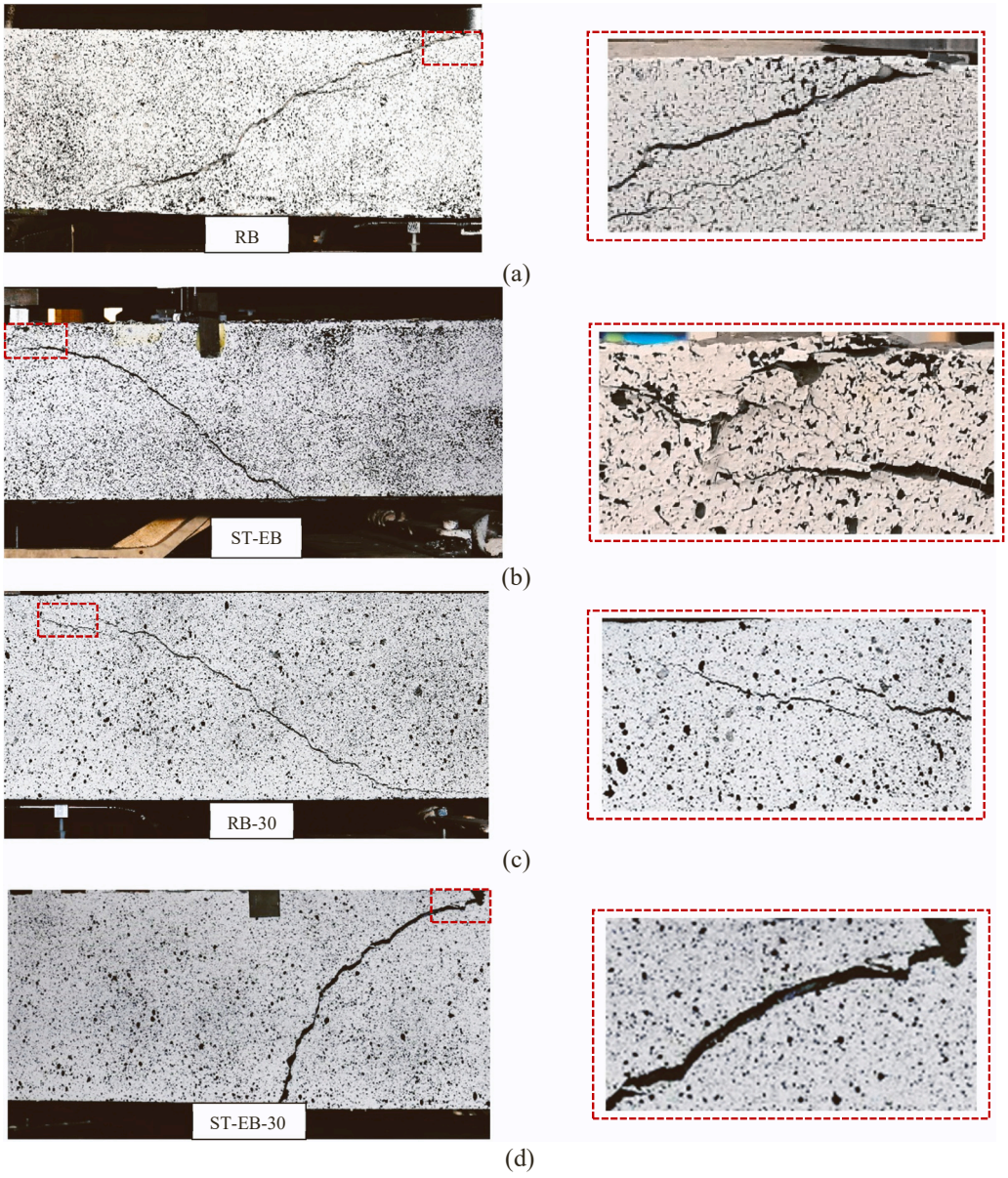

Fig. 13. Crack pattern at failure of test beams with a zoomed view (right): (a) RB; (b) ST-EB; (c) RB-30; (d) ST-EB-30.

even after the beam failure. It is concluded that an effective bonding quality between UHPFRC and NC could be provided with the use of epoxy resin.

5. Numerical investigation

Apart from the experimental investigation, the numerical study is also conducted with the aim to better understand the mechanisms governing the shear response of the strengthened beam with UHPFRC. The commercial finite element software ATENA 3D is used. It should be noted that the effect of freeze-thaw is not numerically investigated since there is negligible concrete strength loss and no obvious damage for ST-EB-30 specimen after experiencing 30 FT cycles, as presented in Table 2 and discussed in Section 4.

5.1. Constitutive material and geometric models

For the material modelling, a fracture-plastic model, named SBETA constitutive model has been used to describe the tensile and compressive behaviour of concrete and UHPFRC. For NC, the compressive strength, elastic modulus and splitting tensile strength as

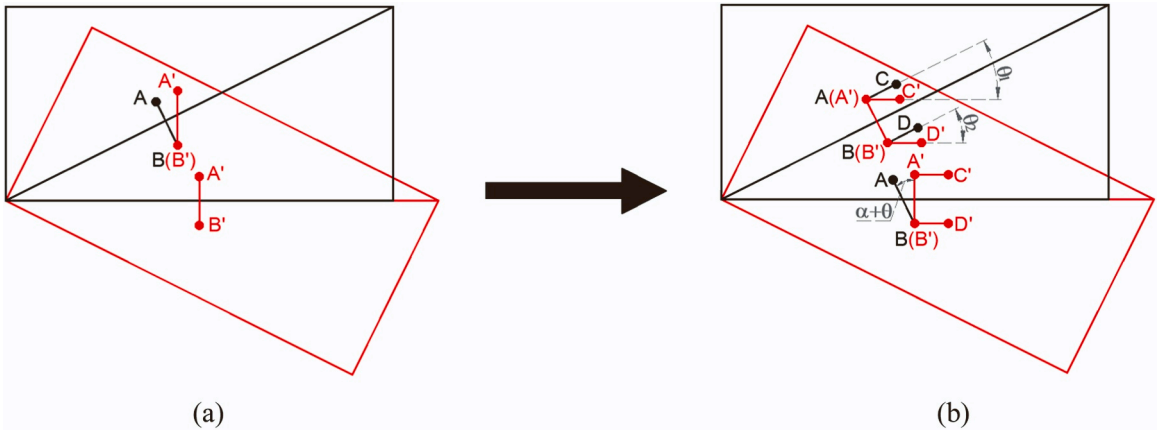

Fig. 14. Crack displacement calculation: (a) 2-point reference system; (b) 4-point reference system.

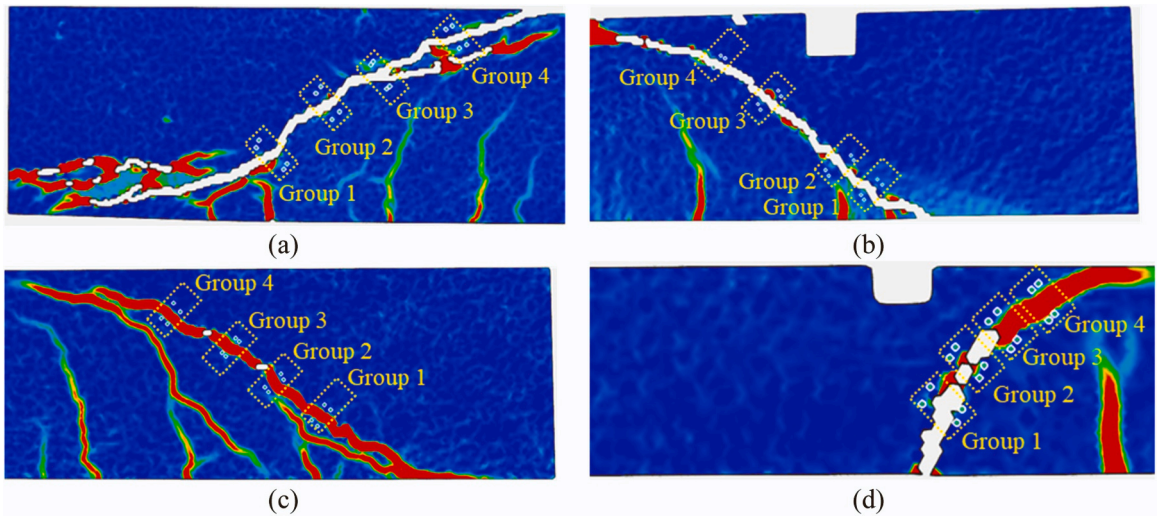

Fig. 15. Crack opening and slip measurement from the 4-point reference system: (a) RB beam; (b) ST-EB beam; (c) RB-30 beam; (d) ST-EB-30 beam.

listed in Table 2 are used as input parameters. For UHPFRC, compressive strength of 120 MPa and elastic modulus of 45 GPa are used. To take into account the effect of fibers, the tensile stress-strain relationship of UHPFRC is defined as presented in Fig. 19. A bilinear relationship is used to simulate the tensile stress-strain behaviour of UHPFRC until the peak tensile strength (i.e. linear elastic phase and strain hardening phase) and the input is calibrated within the scatter obtained in experimental results. In the post-peak phase, the softening part is assumed to be bilinear descending following the trend of stress-crack opening displacement tensile test results. Furthermore, the bilinear stress-strain function with the elastic modulus of 200 GPa and a yield stress of 550 MPa is employed to characterize the rebars.

After material property is defined, 3D FE model for reference and strengthened beam with UHPFRC is built. Since the thickness of UHPFRC strengthening layer is only 10 mm, 8-node 3D hexahedral elements with 10 mm mesh size for the UHPFRC and NC are employed. The steel bars are simulated using discrete reinforcement. Two supports are modelled as hinged and roller supports. Both supports and loading plate are simulated as steel elements with linear stress-strain relation. The loading and support plates used in the experiment are relatively small (as shown in Fig. 6 and Fig. 7), which leads to high stress concentrations causing convergence issues. Therefore, for the numerical stability of the simulations, loading and support plates with a length of 100 mm and a thickness of 20 mm are applied. For simplicity, perfect bond is assumed between the rebars and the NC. Moreover, given that experimental observations on interface (Section 4.3) indicate that there is no debonding between UHPFRC and NC when epoxy bonding is used, the perfect bond is modelled. The test is performed under deformation control, with loading rate of 0.15 mm per load step. The corresponding reaction force and deformation are monitored at the mid-span of the beam. Newton-Raphson method is used to solve the set of nonlinear equations.

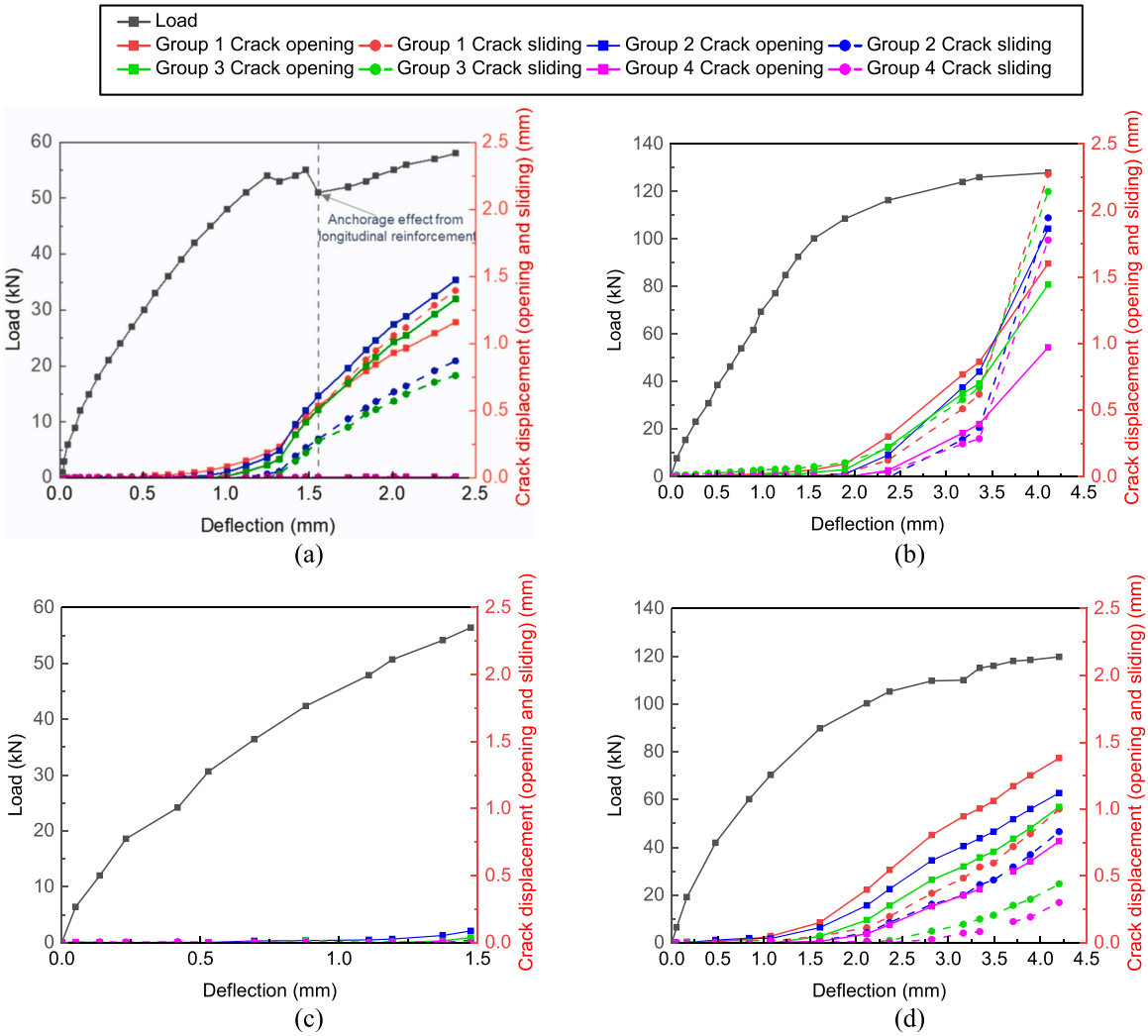

Fig. 16. Crack opening and slip for test beams: (a) RB; (b) ST-EB; (c) RB-30; (d) ST-EB-30.

5.2. *Verification against experimental results*

The comparison of the numerical results with the respective experimental results for RB and ST beams is shown in Fig. 20. The maximum load for both control and strengthened specimens obtained experimentally and numerically is shown in Table 6. It can be observed that the numerical and experimental results are, in general, in good agreement and therefore, validate the effectiveness of the 3D FE model in capturing structural behaviours of the NC-UHPFRC composite beams. The peak load and the trend of load-deflection response for both RB and ST beams are similar. However, compared to experimental results, both RB and ST beams, show a higher simulated stiffness. For RB beam, the underestimation of simulated deflection compared to experimentally measured one might be attributed to using the perfect rebar-concrete bond and neglecting the shrinkage in modelling approach [62]. For ST beam, a stiffer numerical prediction might also result from the properties of UHPFRC. In FE modelling, UHPFRC is always assumed homogenous. However, in reality, there will be flaws during the casting, and inhomogeneous fiber distribution. Therefore, the uniform UHPFRC material properties assumption might lead to an overestimation of stiffness, especially for unreinforced (like in this study) or under-reinforced UHPFRC laminates, as also observed by Feng [63]. Moreover, the FE model does not reliably capture the ductility observed in the experiment, which might be owing to the perfect bond assumption between UHPFRC and NC [64], as also further discussed (Section 5.3). In Fig. 21, the experimentally obtained principal strain contours and numerically predicted crack pattern of RB and ST beams at the ultimate load are presented. It can be seen that for both the RB and ST beams, the main crack is a diagonal shear crack which initiates within the region between the loading point and support. Comparison of experimental and numerical failure patterns of RB and ST beams shows that crack patterns in the numerical model provide a reasonable consistency with the test beams (Fig. 21). It should be emphasized that for better visualization purposes, only the cracks with crack width larger than 0.1 mm are shown in FE modelling.

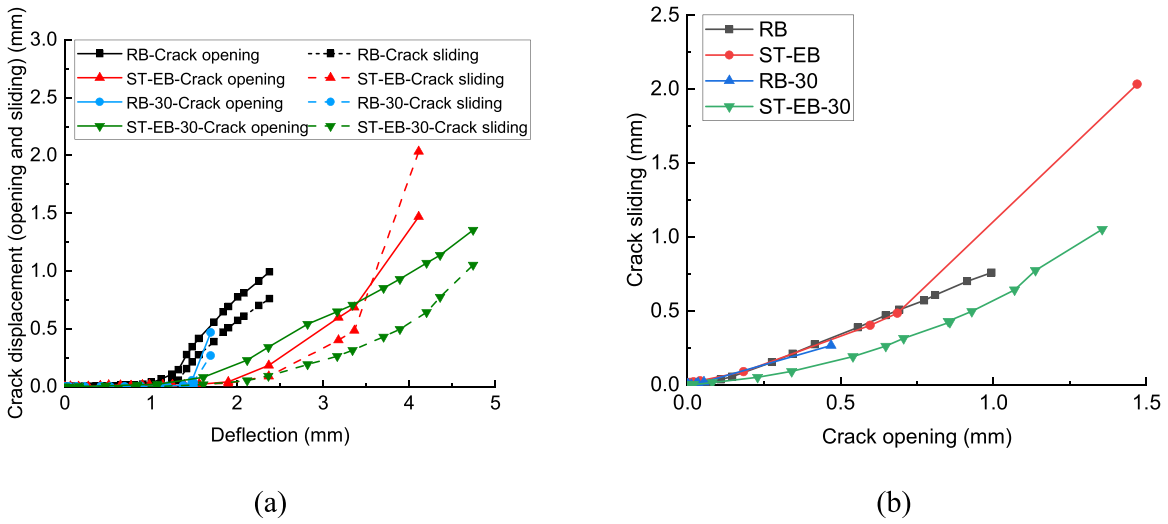

Fig. 17. (a) Crack opening and slip with respect to the deflection and (b) comparison of crack opening-sliding relationship for the major shear crack of RB and ST beam.

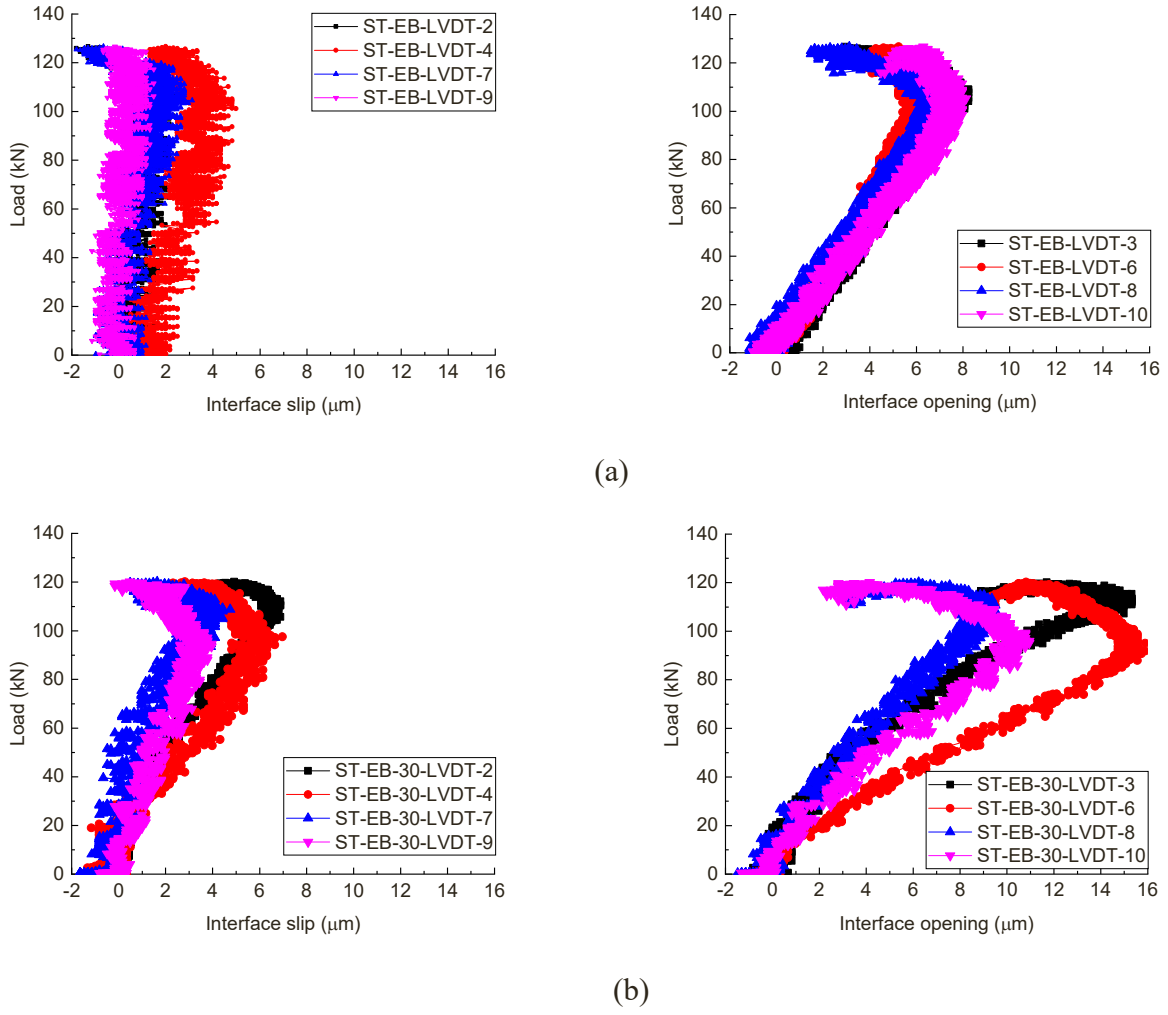

Fig. 18. Interface displacement (slip and opening) measurement for strengthened beam: (a) ST-EB specimen; (b) ST-EB-30 specimen.

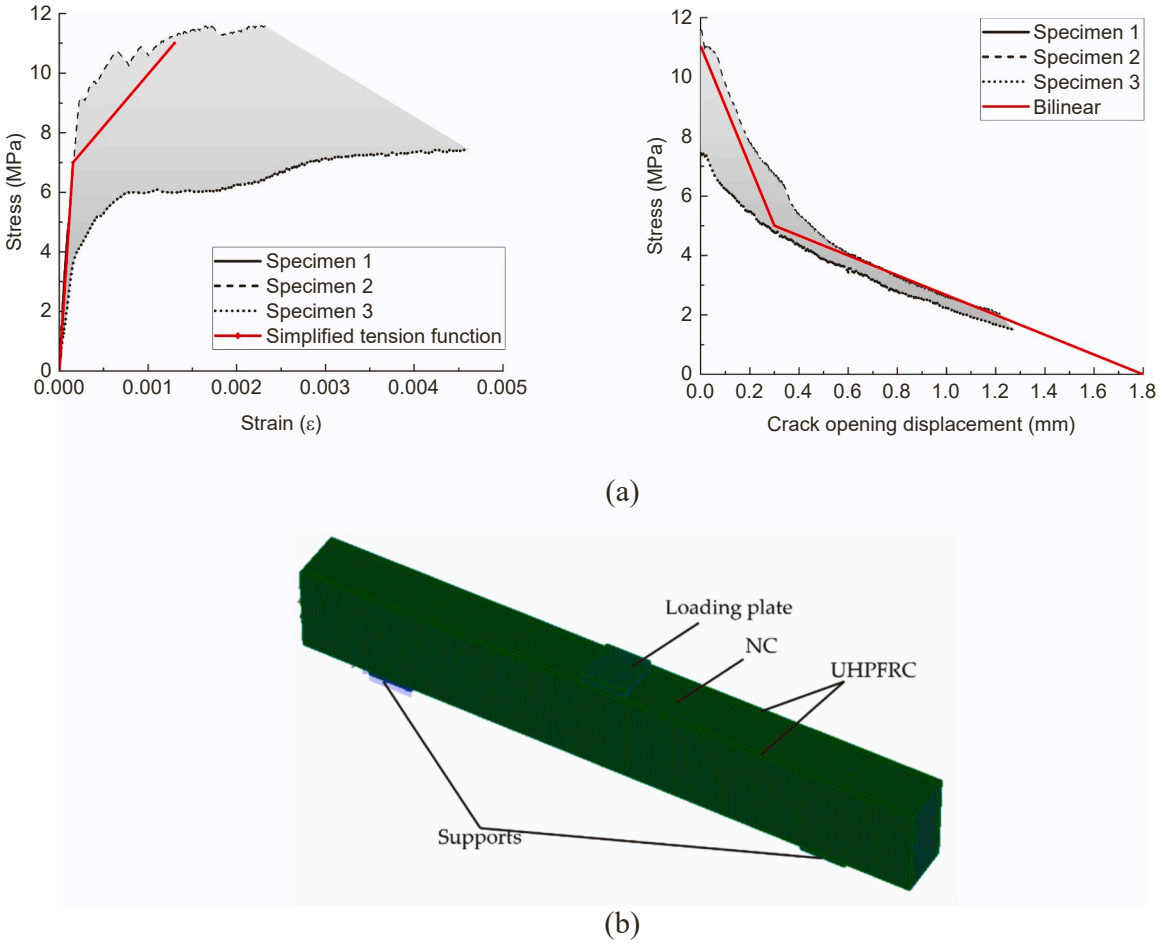

Fig. 19. Numerical model for hybrid beam: (a) simulated simplified tension function along with the tested tensile response for UHPFRC; (b) FE model.

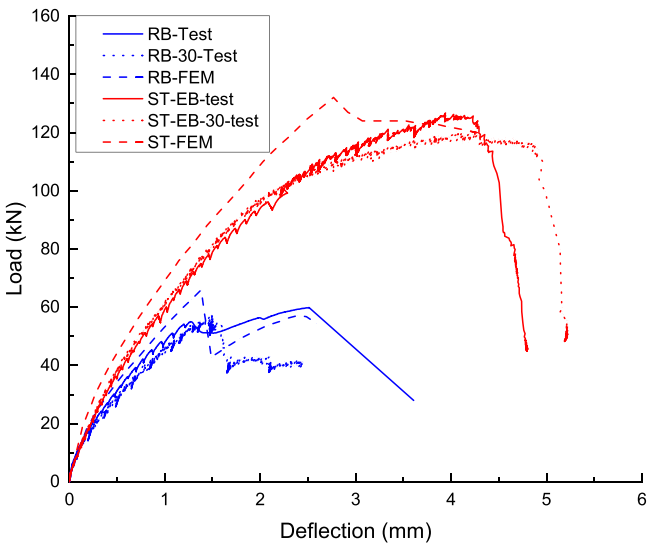

Fig. 20. Comparison between the numerical and experimental results for RB and ST beams.

Table 6
Experimental and simulated maximum load.

Specimen	P_{FEM} (kN)	Δ_{FEM} (mm)	P_{EXP} (kN)	Δ_{exp} (mm)	P_{FEM}/P_{EXP}	$\Delta_{FEM}/\Delta_{exp}$
RB	65.9	1.38	59.8	2.51	1.10	0.55
RB-30			57.3	1.48	1.15	0.93
ST-EB	132	2.77	126.7	3.94	1.04	0.70
ST-EB-30			119.7	4.19	1.10	0.66

5.3. The role of governing parameters

One of the primary goals of the current study is to evaluate the shear strengthening efficiency of concrete beams composited with epoxy-bonded precast UHPFRC laminates under FT action, especially focusing on the effect of FT cycles on the mechanical properties of strengthening material (UHPFRC in this study) and the bond between UHPFRC and concrete. However, due to negligible damage after exposed to 30 FT cycles, both the mechanical properties of UHPFRC and the bond at the interface do not show signs of degradation, thereby the shear capacity of the strengthened beam does not reduce after FT cycles. While previous studies have shown that if the beams are exposed to sufficient freeze thaw cycles, the properties of UHPFRC will be degraded [65,66] and the bond at the interface between UHPFRC and normal concrete will be weakened [67]. Therefore, assuming that the damage occurs after the FT action, a parametric study focusing on the material properties of UHPFRC and the properties of interface is conducted.

In terms of material properties of UHPFRC, the tensile behaviour of UHPFRC is one of the governing parameters for the shear performance of strengthened structures and FT cycles have obvious influence on the tensile properties of UHPFRC, especially in the strain softening branch [66]. Moreover, it is generally accepted that the peak tensile strength and strain hardening capacity of UHPFRC will influence the shear behaviour but the influence of UHPFRC's strain softening phase is still not extensively studied. Therefore, the strain softening branch of UHPFRC is selected for parametric analysis.

In addition, bond conditions at the interface are also numerically investigated and the interface strength and stiffness are mainly varied. Assuming that the bond is weakened after FT cycles, the bond strength is varied to investigate its effect on the shear behaviour of strengthening system. Thereafter, the epoxy resin used in current study could provide enough bond strength and varying the interface stiffness could help to understand the influence of elastic modulus of epoxy resin on the shear behaviour of strengthened structures and provide the recommendation for epoxy resin selection in practice.

Therefore, the role of softening branch of UHPFRC in tension and the interface properties between UHPFRC and NC are studied in current section in order to understand better the fracture behaviour and try to optimize the behaviour of UHPFRC strengthened structures.

5.3.1. The effect of softening branch of UHPFRC

The tensile response of UHPFRC until the peak strength (i.e. linear elastic and strain hardening phase) directly influences the structural response of simulated beams while the strain softening phase is reported to have influence only after the formation of macro-crack of the beams in flexure [68,69]. Since the load when the macro-crack forms nearly approaches the peak load of concrete structures failing in shear, the softening phase might have a minor role in shear-critical concrete members without shear reinforcement. However, as discussed in Section 4.2, due to the bridging effect of steel fibers in UHPFRC, the load can still be transferred after the formation of macrocrack. Therefore, a parametric study for the softening behaviour of UHPFRC is conducted in which the shape of descending branch and the ultimate crack opening limit are varied, assuming the same tensile behaviour for linear elastic and strain hardening phases.

Generally, the softening branch of UHPFRC is assumed either linear or bi-linear for ultimate load prediction [70]. Therefore, apart from the bilinear softening curve as defined in Fig. 19 (a), another three linear softening functions are assumed, as presented in Fig. 22. The first one simply neglects the contribution of softening branch of UHPFRC with a rapid decreasing linear curve (referred to as Linear - w_u=0.05 mm). The second one has a slope of descending branch keeping the same as the initial descending slope obtained from the tensile test results (and referred to as Linear - w_u=0.25 mm). For the third softening function, similar ultimate crack opening (w_u) is assumed as observed in the direct tension test (referred to as Linear - w_u=1.8 mm).

The simulated load-deflection response of hybrid beams with assumed softening functions, along with numerical-to-experimental peak load ratio (P_{FEM} / P_{EXP}) and ductility ratio (Δ_{FEM} / Δ_{EXP}) is shown in Fig. 23. From the load-deflection response, it is found that all the simulations show higher stiffness than the tested results and the peak load is well predicted (within 10% error) for all the assumed softening functions. The softening branch of UHPFRC has a negligible effect on the peak load and deflection if a reasonable softening input is given, which is evidently observed in simulated results among Linear - w_u= 0.25 mm, Bilinear and Linear - w_u= 1.8 mm. However, if the softening branch of UHPFRC is not taken into consideration as represented by softening function linear - w_u= 0.05 mm, lower simulated peak load and deflection are obtained as the contribution of fracture energy of the UHPFRC is greatly underestimated. In addition, it can be clearly seen that the softening branch of UHPFRC will mainly influence the post-peak behaviour of the hybrid structure. For deformation prediction, although the ductility at the peak load is not appropriately captured with any of the assumed softening functions, the linear function with w_u= 1.8 mm input shows the closest deflection capacity to the experiments (Δ_{FEM} / Δ_{EXP} equals 0.74). The simulated cracking patterns at failure for the assumed softening functions are presented in Fig. 24 and it can be seen that the beams with all assumed softening functions show similar shear failure modes as observed in the experiment. Therefore, the UHPFRC softening part has little role in the failure patterns.

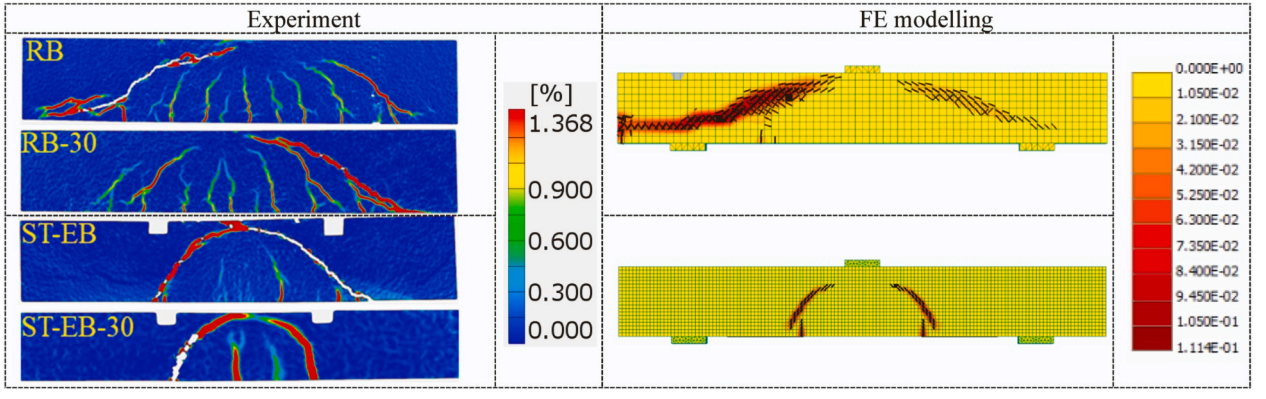

Fig. 21. Crack pattern at the peak load for RB and ST beam.

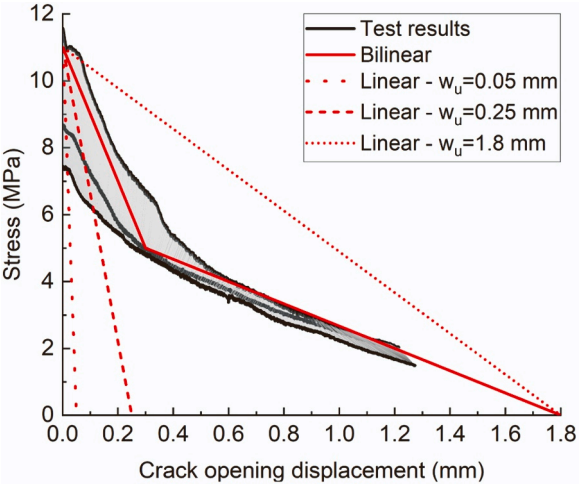

Fig. 22. Assumed three softening functions of UHPFRC in tension.

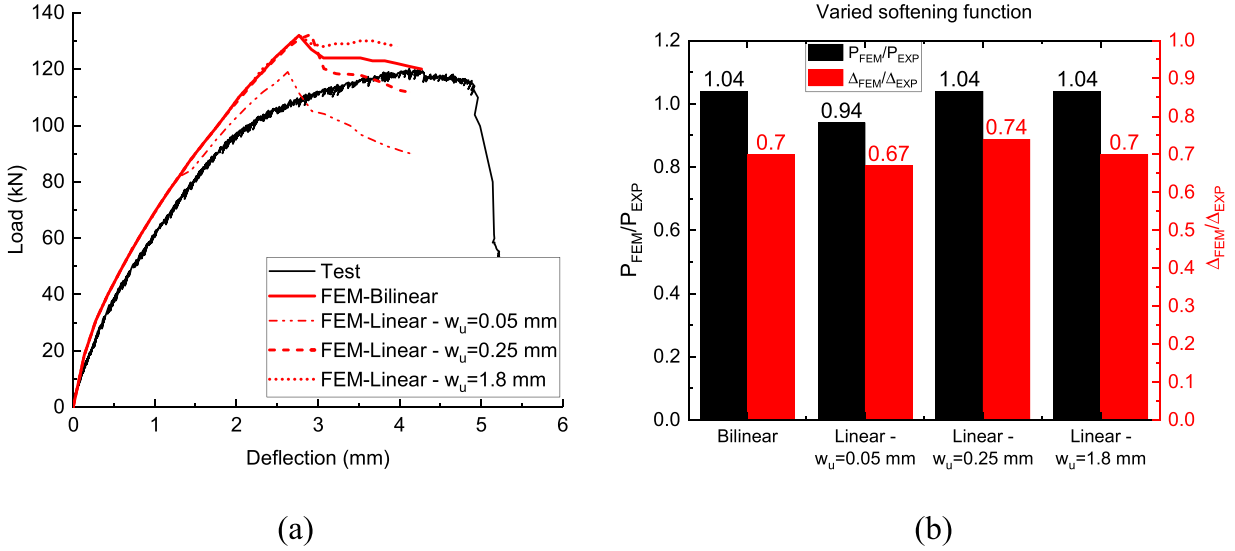

Fig. 23. Comparison between experimental and simulated results with different softening functions of UHPFRC: (a) Load-deflection response, (b) peak load ratio (P_{FEM} / P_{EXP}) and ductility ratio (Δ_{FEM} / Δ_{EXP}).

5.3.2. The effect of interface properties

Based on the experimental results, perfect bond assumption is made in FE modelling as high bond strength between UHPFRC and normal concrete could be guaranteed with epoxy resin bonding. However, improper interface preparation, inappropriate curing condition and severe environment will easily lead to debonding of the composite UHPFRC-NC specimen. Since interface behaviour plays a significant role on the structural performance of UHPFRC-NC specimens, it is worthwhile to investigate the influence of interface strength on the strengthening effect with the application of UHPFRC.

The ATENA interface material model, in which interface element is regarded as a zero-thickness element, provides the possibility to simulate the contact between UHPFRC and concrete. As shown in Fig. 25, the interface model is based on Mohr-Coulomb failure criterion with tension cut-off, and typical interface behaviour in tension and shear, which leads to the opening and sliding displacement respectively at the interface. The main parameters to characterize the interface behaviour are normal and tangential stiffness K_{nn} and K_{tt}, tensile strength f_t, cohesion C and coefficient of friction μ at the interface. Minimum normal and tangential stiffness $K_{nn}^{\min}$ and $K_{tt}^{\min}$ are adopted for the numerical purpose, and normally are 0.1% of the initial normal and tangential stiffness K_{nn} and K_{tt}, respectively.

Previous research by Valikhani [72,73] is used to define the parameters for the interface strength between UHPFRC and NC (Table 7). The strengthened concrete beams with UHPFRC considering "weak bond" and "strong bond with high interface stiffness (SBHS)" are defined. In addition, in order to study the effect of interface stiffness, interface parameters for "strong bond with low

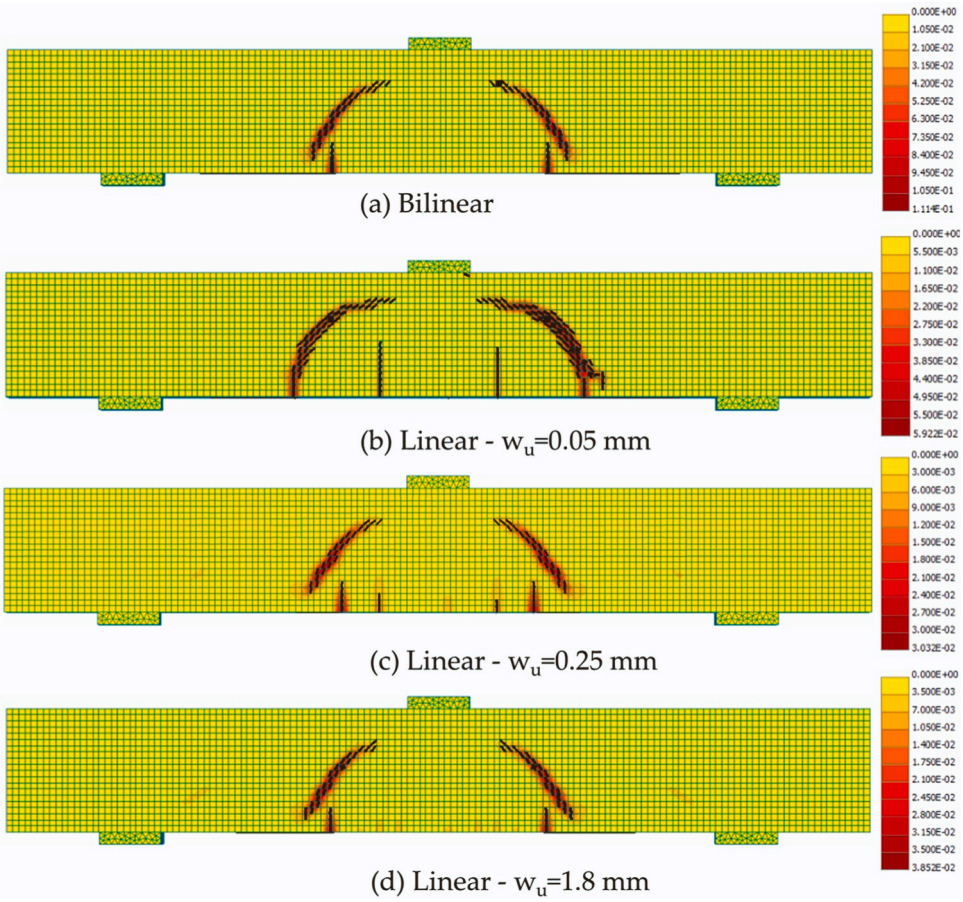

Fig. 24. Final failure patterns for the assumed softening function in FE modelling.

stiffness (SBLS)" and "strong bond with medium stiffness (SBMS)" are assumed. SBLS is introduced by combining f_t, C and μ from SBHS and interface stiffness (K_{nn}, K_{tt}, $K_{nn}^{\min}$ and $K_{tt}^{\min}$) from "weak bond". SBMS is defined by the samef_t, c and μ while the stiffness is assumed ten times higher than "weak bond".

Fig. 26 shows the simulated load-deflection curves together with numerical to experimental peak load and ductility ratio. Varying bond properties influences both the peak load and the ductility of the beam, but the initial stiffness remains unchanged. The numerical-to-experimental peak load ratio (P_{FEM} / P_{EXP}) decreases if a weak bond or "SBHS" is provided when compared to the hybrid beam with perfect bond. With a higher capacity than "SBHS", "SBMS" and "SBLS" show almost the same shear capacity as that of the perfect bond assumption which ensures monolithic action of UHPFRC and concrete. For the deformation capacity, "SBMS" and "SBLS" show a more ductile response compared to perfect bond assumption while weak bond leads to brittle failure due to premature delamination between UHPFRC and NC. Therefore, not only the bond strength, the interface stiffness also plays a significant role both in the peak load and ductility of the strengthened beam, which is evident when the load-deflection responses of the strong bond with varying interface stiffness are compared. However, the relationship is not linear. A possible reason for the effect of interface stiffness might be that assuming the same bond failure criteria (i.e.f_t, C and μ are the same), higher interface stiffness leads to localized delamination at lower loads. As a result, a more severe stiffness degradation and a reduced peak load in load-deflection behaviour of "SBHS" are obtained. An interface with low stiffness (such as in "SBLS" or "SBMS") allows a larger interface displacement before failure, and helps to keep the specimen intact.

In order to provide a deeper insight into the role of interface properties, the final failure patterns both in UHPFRC laminates and RC section, as well as the interface shear displacement after the peak load are given in Fig. 27. When a weak bond strength is modelled, the failure pattern is not compatible in UHPFRC laminate and RC section (seen in Fig. 27 (a)) since the debonding between UHPFRC and normal concrete happens at lower load levels instead of shear failure, as validated by a considerable interface shear displacement shown in Fig. 27 (b). For "SBLS" models, the bond strength is sufficient to resist the debonding stress at the interface resulting in shear failure. While for "SBMS", the shear crack is not fully developed in UHPFRC layers though similar peak load is achieved compared to "SBLS", which is attributed to the localized delamination around the shear cracking area in composite beams. The delamination also occurs for "SBHS" after the peak load, which is caused by the splitting crack developing along the tensile rebar in RC part of the composite beam. Although the effect of the failure envelope is straightforward (lower bond strength might lead to early debonding and

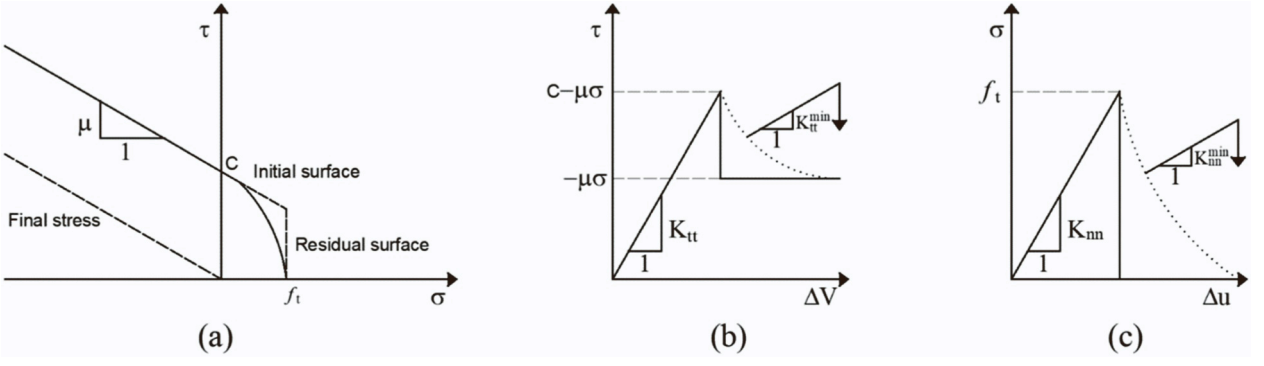

Fig. 25. Interface material model: (a) Mohr-Coulomb failure criteria with tension cut-off, (b) interface behaviour in shear and (c) interface behaviour in tension [71].

Table 7
Interface parameters for simulated weak and strong bonds with varied interface stiffness.

Interface bond type	f_t (MPa)	C (MPa)	μ	K_{nn} (MN/m^3)	K_{tt} (MN/m^3)	K_{nn}^{min} (MN/m^3)	K_{tt}^{min} (MN/m^3)
Weak bond	0.5	2.8	0.5	10^6	10^6	10^3	10^3
SBHS	2	6.28	1	2.2×10^8	2.2×10^8	2.2×10^5	2.2×10^5
SBMS	2	6.28	1	10^7	10^7	10^4	10^4
SBLS	2	6.28	1	10^6	10^6	10^3	10^3

Note: SBHS, SBMS, SBLS are denoted as “strong bond with high interface stiffness”, “strong bond with medium stiffness” and “strong bond with low interface stiffness” respectively.

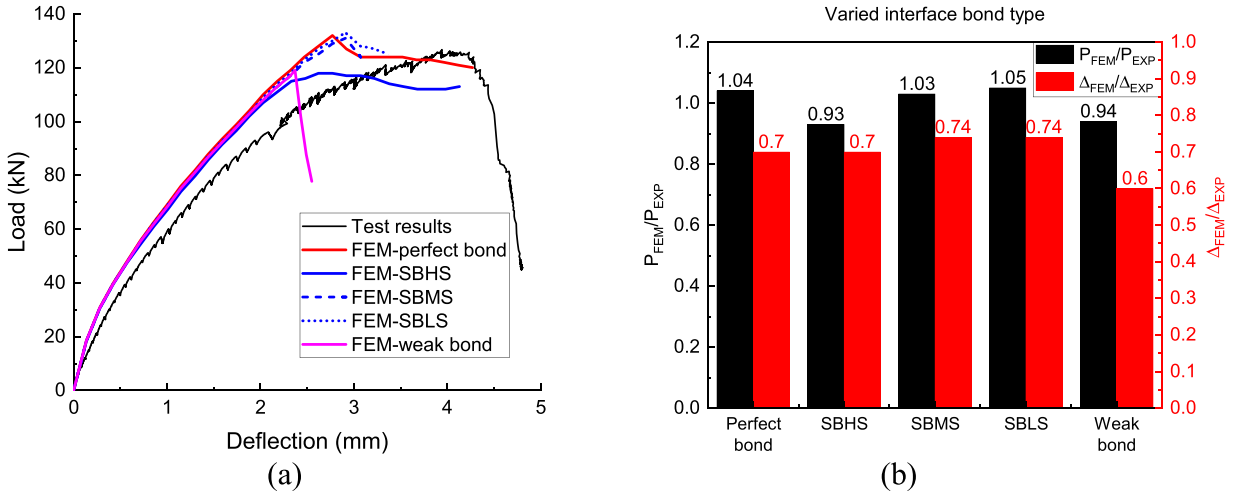

Fig. 26. Comparison between experimental and simulated results with different interface properties: (a) Load-deflection response, (b) peak load ratio (P_{FEM} / P_{EXP}) and ductility ratio (Δ_{FEM} / Δ_{EXP}).

therefore lower capacity), the role of interface stiffness is still not fully understood. It is clear that lower stiffness might be beneficial, but a more in-depth study on the relationship between interface stiffness, fracture propagation and structural response (such as peak load, ductility and failure pattern) is required.

6. Discussion

Based on the experimental and numerical studies, it is found that UHPFRC shows great potential to increase the shear capacity of RB beams without transverse reinforcement if a good bond quality between UHPFRC and concrete is provided. Epoxy bonding of prefabricated UHPFRC laminates on the shear-deficient concrete beam is a suitable technique to guarantee the strengthening effect without debonding. However, it should be noted that the success of epoxy-bonded techniques is dependent on various factors, such as types of epoxy adhesives [74], curing conditions [75,76], surface preparation of concrete substrate [77–79], as well as the thickness of epoxy layer [80]. There are findings summarized in [29] that in some cases, the epoxy resin even undermines the bond quality, which is possibly caused by the following reasons. Firstly, epoxy is more effective to increase the bond strength between two dry hardened concretes when compared to wet-dry concrete bond because moisture is detrimental to epoxy-concrete interface [81]. Secondly, the surface roughness also affects the bond strength with the use of epoxy-based bonding agent and it is found that the bond will be enhanced in smooth surface and weakened in relatively rough surface of concrete substrate. The possible reason is that the epoxy will reduce the effective contact area between the strengthening material and concrete substrate, which reduces the cohesion at the interface [78]. Finally, when epoxy resin is exposed to severe environment such as high temperature or humidity [82], its mechanical properties will degrade, which finally leads to the failure of its application. Therefore, in current study, a commercial epoxy resin Sikadur®– 30, which could provide strong bond, is applied to a prepared dry and smooth concrete surface. Subsequently, the epoxy resin is cured under appropriate lab condition to ensure that the bond strength is properly developed. Although one strengthened beam is subjected to freeze thaw cycles, the bond quality is not obviously damaged since it is exposed to a maximum temperature of around 20 degrees, the relative humidity between 50% and 70%, and the number of freeze thaw cycles is limited to 30. However, the challenges to bond with the application of such type of epoxy still exist when it is applied to large-scale concrete members exposed to harsher environment condition, which requires further investigation.

Experimental study shows that the epoxy resin bonding technique could also keep the composite beam intact when exposed to 30 FT cycles and subsequently loaded. Note that the applied freeze-thaw regime, conducted under a humidity ranging from 50% to 70%, is less harsh than the commonly applied FT test [83], in order to imitate the environmental condition that in-service concrete structures

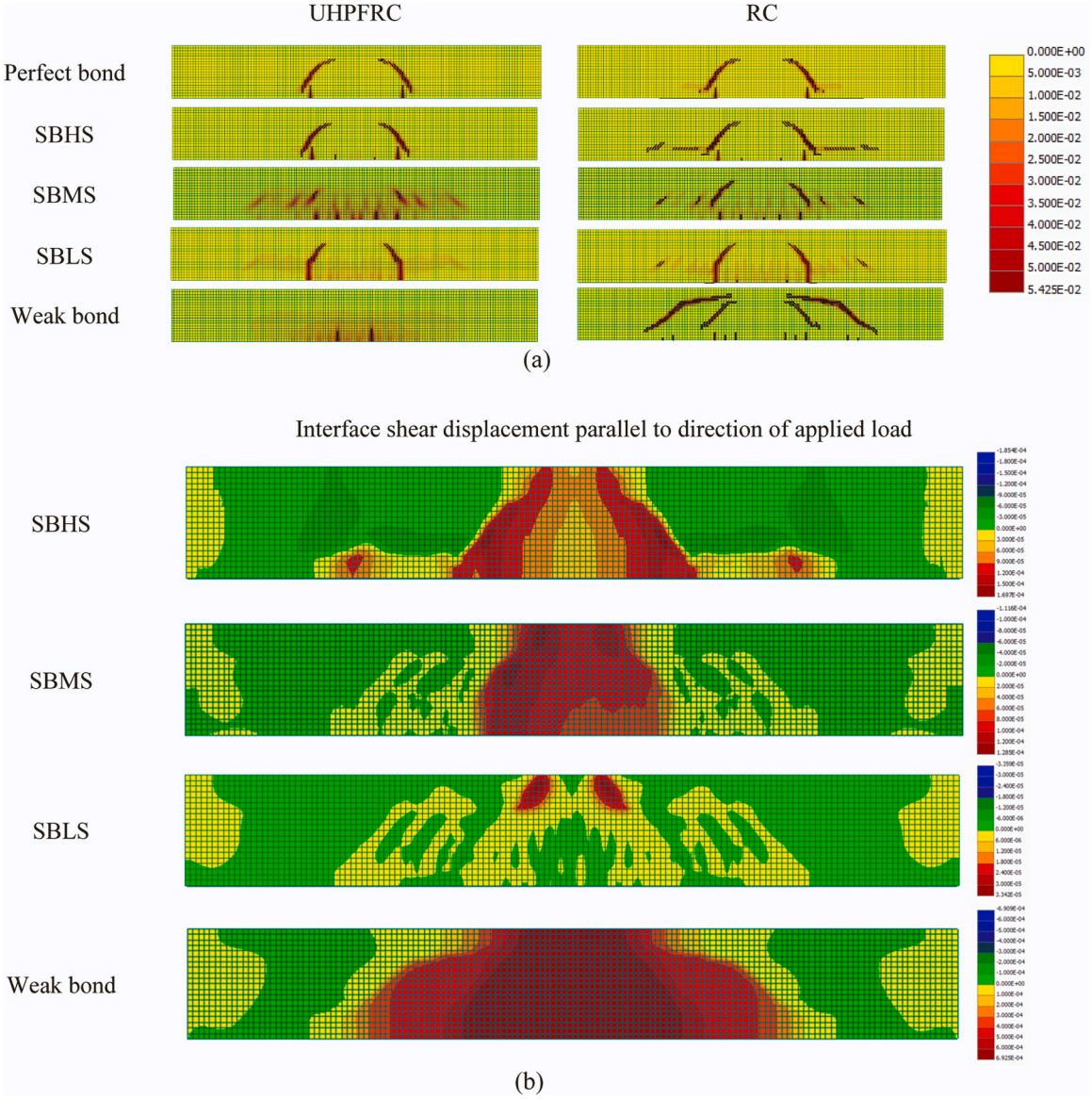

Fig. 27. Final failure patterns (both in UHPFRC laminate and RC part) and interface shear displacement for different interface properties in FE modelling: (a) Failure pattern in UHPFRC and RC respectively; (b) interface shear displacement immediately after peak load.

are exposed to. The moisture content in concrete will govern the freeze-thaw resistance since compressive and tensile stress induced by the volumetric change of water in voids will lead to crack formation and propagation [84]. In addition, the study is focused on investigating the effect of FT action in the first one/two years of the strengthening application so 30 FT cycles are employed. From the results this number of FT cycles is found to be insufficient to cause structural degradation. It is difficult to predict the number of FT cycles that would lead to the damage of the strengthened beams due to the following reasons. Firstly, although many codes or standards such as ASTM C666/C666M [85], GB/T 50082–2009 [86] or CEN/TR 15177 [87] define the testing protocol to assess the freeze thaw resistance of concrete material, the mechanisms and rate of damage might differ in RC structures where steel reinforcement and interfaces are also present in concrete. Currently, there is no universal testing method for the structural performance of RC members. Secondly, due to the differences in specified exposure conditions, the number of FT cycles is varied in existing standards, for example, 300 cycles in ASTM C666/C666M, minimum 25 cycles in GB/T 50082–2009 and 56 cycles in CEN/TR 15177. Finally, compared to conventional concrete, UHPFRC can sustain more FT cycles [88] due to its denser microstructures and UHPFRC-concrete bond is also reported to be stronger than the concrete-concrete bond due to the existence of fibers [30], leading to higher resistance to FT action. Therefore, more FT cycles and/or harsher conditions such as higher moisture levels or submersion in water environment should be applied in further studies to evaluate the robustness of the epoxy-bonded UHPFRC strengthening system.

A negligible interface displacement in all tested beams is observed. However, applied LVDT measurements are limited only to

several points at the interface. The interaction between concrete and UHPFRC along the whole interface area and possible (local) debonding could not be captured. Therefore, the next step should be focused on using Digital image correlation or infrared thermography for the quantitative study of interface behaviour along the whole interface length.

Furthermore, it should be noted that the geometry and proportions of the beam in the current study are not realistic (beam size is much smaller than representative beams in existing structures), which can have a significant effect on the shear behaviour). The role of size effect and possible benefits of shear strengthening with UHPFRC for deep beams should be studied in the future.

From the numerical study it is observed that the fractural behaviour of UHPFRC and interface plays a role in shear strengthening efficiency. A proper softening relationship of UHPFRC is required to provide reasonable prediction of the structural response of UHPFRC composite. In addition, both the bearing capacity and fracture pattern are influenced by interface properties. Therefore, in order to realistically capture the structural response for the composite UHPFRC-NC members considering the interface, the challenge to characterize the real interface behaviour between UHPFRC and NC still exists.

7. Conclusion

In order to investigate the shear performance of reinforced concrete beams strengthened with UHPFRC, combined experimental and numerical studies have been carried out. Tests were conducted to determine the material properties of UHPFRC and normal concrete. The strengthening effect of epoxy-bonded prefabricated UHPFRC lamellas on shear-deficient beams is evaluated. Prior to mechanical tests, some beams were subjected to freeze-thaw cycles. Based on the experimental and numerical results, the following conclusions could be drawn:

1. With the precast UHPFRC panels applied on lateral sides of the shear-deficient reinforced concrete beam by epoxy resin, an increase of 112% and 57% for loading and deflection capacity, respectively, were found. This proves that reinforced concrete structures strengthened with UHPFRC is a promising method to enhance their shear resistance. In addition, a negligible decrease (around 5%) in loading capacity is found for both the RB and strengthened concrete beams with UHPFRC subjected to 30 FT cycles, being in line with compressive strength measurements.
2. A 4-point reference system is proposed to eliminate the effect of rigid body rotation and calculate the shear crack displacement. Based on the calculated results, it is found that the shear crack first opens and subsequently starts sliding for both RB and ST beams. In addition, for ST beam, the crack opening and sliding significantly reduce due to the bridging effect of steel fibers inside the UHPFRC. Finally, UHPFRC enables a certain residual bearing capacity when shear crack is visually observed.
3. Whether or not freeze-thaw action is applied, negligible interface slip and opening are measured, proving that bonding UHPFRC with epoxy resin is an effective technique to provide robust system. Once the critical shear crack is initiated, the interface opening and slip will start decreasing, which can be also an indication of the final failure.
4. From the numerical study of the UHPFRC tensile behaviour, and more specifically softening region, it is found that the softening of UHPFRC mainly affects the post-peak behaviour of concrete beam strengthened with UHPFRC in shear. Note that the peak load and deformational capacity are underestimated if the contribution of softening branch (i.e. fracture energy) of UHPFRC is not considered.
5. The interface properties is one of the most important parameters affecting the shear strengthening efficiency of UHPFRC. Through the numerical study, it is found that both the bond strength and the interface stiffness will affect significantly the load capacity, ductility and failure patterns. Without proper interface design, the composite structure will partially or fully delaminate at low load levels and enhanced shear performance cannot be activated, greatly weakening the benefits of UHPFRC strengthening in shear.

Declaration of Competing Interest

The authors declare that they have no known competing financial interests or personal relationships that could have appeared to influence the work reported in this paper.

Data availability

Data will be made available on request.

Acknowledgements

This work was supported by the Dutch Organization for Scientific Research (NWO) under the grant “Optimization of interface behaviour for innovative hybrid concrete structures” (project number 16814). Yitao Huang would like to acknowledge the funding support from China Scholarship Council (CSC) under the grant CSC No. 201906950087. Support from our colleagues Hayo Hendrikse and Cody Owen during the Freeze-thaw test is also greatly appreciated.

References

[1] K. Habel, M. Viviani, E. Denarié, E. Brühwiler, Development of the mechanical properties of an Ultra-High Performance Fiber Reinforced Concrete (UHPFRC), Cem. Concr. Res 36 (2006) 1362–1370, https://doi.org/10.1016/J.CEMCONRES.2006.03.009.

[2] R. Yu, P. Spiesz, H.J.H. Brouwers, Mix design and properties assessment of Ultra-High Performance Fibre Reinforced Concrete (UHPFRC, Cem. Concr. Res 56 (2014) 29–39, https://doi.org/10.1016/J.CEMCONRES.2013.11.002.
[3] E. Fehling, M. Schmidt, J. Walraven, T. Leutbecher, S. Fröhlich, Ultra-High. Perform. Concr. UHPC (2014).
[4] M. Schmidt, D. Jerebic, UHPC: basis for sustainable structures-the Gaertnerplatz bridge in Kassel, Ultra High. Perform. Concr. 2 (2008) 5–7.
[5] T. Yoshihiro, K. Maekawa, Y. Kameyama, A. Ohtake, H. Musha, N. Watanabe, Innov. Appl. UHPFRC Bridges Jpn. (2011) 149–188, https://doi.org/10.1002/9781118557839.ch12.
[6] T. Noshiravani, E. Brühwiler, Experimental investigation on reinforced ultra-high-performance fiber-reinforced concrete composite beams subjected to combined bending and shear, Acids Struct. J. 110 (2013) 251–261, https://doi.org/10.14359/51684405.
[7] E. Brühwiler, E. Denarié, Rehabilitation and strengthening of concrete structures using ultra-high performance fibre reinforced concrete, Struct. Eng. Int J. Int Assoc. Bridg Struct. Eng. 23 (2013) 450–457, https://doi.org/10.2749/101686613×13627347100437.
[8] M. Bastien-Masse, E. Brühwiler, Contribution of R-UHPFRC strengthening layers to the shear resistance of RC elements, Struct. Eng. Int J. Int Assoc. Bridg Struct. Eng. 26 (2016) 365–374, https://doi.org/10.2749/101686616×14555429843924.
[9] S.A. Paschalis, A.P. Lampropoulos, O. Tsioulou, Experimental and numerical study of the performance of ultra high performance fiber reinforced concrete for the flexural strengthening of full scale reinforced concrete members, Constr. Build. Mater. 186 (2018) 351–366, https://doi.org/10.1016/j.conbuildmat.2018.07.123.
[10] M.A. Al-Osta, Exploitation of Ultrahigh-Performance Fibre-Reinforced Concrete for the Strengthening of Concrete Structural Members, Adv. Civ. Eng. 2018 (2018), https://doi.org/10.1155/2018/8678124.
[11] Oesterlee C. Structural response of reinforced UHPFRC and RC composite members, 2010;4848:159. https://doi.org/10.5075/epfl-thesis-4848.
[12] M.A. Sakr, A.A. Sleemah, T.M. Khalifa, W.N. Mansour, Shear strengthening of reinforced concrete beams using prefabricated ultra-high performance fiber reinforced concrete plates: Experimental and numerical investigation, Struct. Concr. 20 (2019) 1137–1153, https://doi.org/10.1002/suco.201800137.
[13] B. Dadmand, M. Pourbaba, R. Riahi, Experimental and Numerical Investigation of Different Types of Jacketing Effect on Retrofitting RC Short Columns Using ECC Concrete, Period Polytech. Civ. Eng. (2022), https://doi.org/10.3311/PPci.19114.
[14] J. Xue, B. Briseghella, F. Huang, C. Nuti, H. Tabatabai, B. Chen, Review of ultra-high performance concrete and its application in bridge engineering, Constr. Build. Mater. (2020), https://doi.org/10.1016/j.conbuildmat.2020.119844.
[15] B. Pan, F. Liu, Y. Zhuge, J.J. Zeng, J.J. Liao, ECCs/UHPFRCCs with and without FRP reinforcement for structural strengthening/repairing: A state-of-the-art review, Constr. Build. Mater. (2022), https://doi.org/10.1016/j.conbuildmat.2021.125824.
[16] Y. Ding, K. Yu, M. Li, A review on high-strength engineered cementitious composites (HS-ECC): Design, mechanical property and structural application, Structures (2022), https://doi.org/10.1016/j.istruc.2021.10.036.
[17] Y. Zhu, Y. Zhang, H.H. Hussein, G. Chen, Flexural strengthening of reinforced concrete beams or slabs using ultra-high performance concrete (UHPC): A state of the art review, Eng. Struct. (2020), https://doi.org/10.1016/j.engstruct.2019.110035.
[18] Y. Huang, S. Grünewald, E. Schlangen, M. Luković, Strengthening of concrete structures with ultra high performance fiber reinforced concrete (UHPFRC): A critical review, Constr. Build. Mater. 336 (2022), 127398, https://doi.org/10.1016/j.conbuildmat.2022.127398.
[19] M. Pourbaba, A. Joghataie, A. Mirmiran, Shear behavior of ultra-high performance concrete, Constr. Build. Mater. (2018), https://doi.org/10.1016/j.conbuildmat.2018.06.117.
[20] T. Mészöly, N. Randl, Shear behavior of fiber-reinforced ultra-high performance concrete beams, Eng. Struct. (2018), https://doi.org/10.1016/j.engstruct.2018.04.075.
[21] Q. Wang, H.L. Song, C.L. Lu, L.Z. Jin, Shear performance of reinforced ultra-high performance concrete rectangular section beams, Structures (2020), https://doi.org/10.1016/j.istruc.2020.07.036.
[22] V. Garg, P.P. Bansal, R. Sharma, Retrofitting of Shear-Deficient RC Beams Using UHP-FRC, Iran. J. Sci. Technol. - Trans. Civ. Eng. (2019), https://doi.org/10.1007/s40996-019-00241-7.
[23] A. Sine, M. Pimentel, S. Nunes, A. Dimande, Shear behaviour of RC-UHPFRC composite beams without transverse reinforcement, Eng. Struct. (2022), https://doi.org/10.1016/j.engstruct.2022.114053.
[24] H. Ji, C. Liu, Ultimate shear resistance of ultra-high performance fiber reinforced concrete-normal strength concrete beam, Eng. Struct. (2020), https://doi.org/10.1016/j.engstruct.2019.109825.
[25] L. Hussein, L. Amleh, Structural behavior of ultra-high performance fiber reinforced concrete-normal strength concrete or high strength concrete composite members, Constr. Build. Mater. (2015), https://doi.org/10.1016/j.conbuildmat.2015.05.030.
[26] A.A. Bahraq, M.A. Al-Osta, S. Ahmad, M.M. Al-Zahrani, S.O. Al-Dulaijan, M.K. Rahman, Experimental and numerical investigation of shear behavior of RC beams strengthened by ultra-high performance concrete, Int J. Concr. Struct. Mater. (2019), https://doi.org/10.1186/s40069-018-0330-z.
[27] M. Alkaysi, S. El-Tawil, Factors affecting bond development between Ultra High Performance Concrete (UHPC) and steel bar reinforcement, Constr. Build. Mater. (2017), https://doi.org/10.1016/j.conbuildmat.2017.03.091.
[28] B.H. Ahangarnazhad, M. Pourbaba, A. Afkar, Bond behavior between steel and Glass Fiber Reinforced Polymer (GFRP) bars and ultra high performance concrete reinforced by Multi-Walled Carbon Nanotube (MWCNT), Steel Compos Struct. (2020), https://doi.org/10.12989/scs.2020.35.4.463.
[29] W.L. Baloch, H. Siad, M. Lachemi, M. Sahmaran, A review on the durability of concrete-to-concrete bond in recent rehabilitated structures, J. Build. Eng. (2021), https://doi.org/10.1016/j.jobe.2021.103315.
[30] Y. Huang, E. Schlangen, M. Luković, Strengthening of reinforced concrete beams with ultra-high performance fiber-reinforced concrete in shear. Int. Symp. Int. Fed. Struct. Concr, Springer,, 2023, pp. 695–705.
[31] Y. Zhu, Y. Zhang, H.H. Hussein, J. Liu, G. Chen, Experimental study and theoretical prediction on shrinkage-induced restrained stresses in UHPC-RC composites under normal curing and steam curing, Cem. Concr. Compos 110 (2020), 103602, https://doi.org/10.1016/j.cemconcomp.2020.103602.
[32] M. Chilwesa, L. Facconi, F. Minelli, A. Reggia, G. Plizzari, Shrinkage induced edge curling and debonding in slab elements reinforced with bonded overlays: Influence of fibers and SRA, Cem. Concr. Compos 102 (2019) 105–115, https://doi.org/10.1016/j.cemconcomp.2019.04.017.
[33] A.P. Lampropoulos, S.A. Paschalis, O.T. Tsioulou, S.E. Dritsos, Strengthening of reinforced concrete beams using ultra high performance fibre reinforced concrete (UHPFRC, Eng. Struct. 106 (2016) 370–384, https://doi.org/10.1016/j.engstruct.2015.10.042.
[34] Bruwer C. Influence of Unidirectional CFRP Plate Pull-Off Strength Bonded To Concrete By Means of Epoxy and a Combination of Epoxy and Mechanical Anchors n.d.
[35] A. Khalifa, T. Alkhrdaji, A. Nanni, S. Lansburg, Anchorage of surface mounted FRP reinforcement, Concr. Int 21 (1999) 49–54.
[36] B. Standard, Testing hardened concrete. Compressive Strength Test Specimens, BS EN (2009) 12390–12393.
[37] Japan Society of Civil Engineers, Recommendations for Design and Construction of High Performance Fiber Reinforced Cement Composites with Multiple Fine Cracks (HPFRCC), Concr. Eng. Ser. (2008).
[38] H. Huang, A. Su, X. Gao, Y. Yang, Influence of formwork wall effect on fiber orientation of UHPC with two casting methods, Constr. Build. Mater. (2019), https://doi.org/10.1016/j.conbuildmat.2019.04.200.
[39] J. Silfwerbrand, Stresses and strains in composite concrete beams subjected to differential shrinkage, Acids Struct. J. 94 (1997) 347–353, https://doi.org/10.14359/485.
[40] J. Zhou, G. Ye, E. Schlangen, K. van Breugel, Modelling of stresses and strains in bonded concrete overlays subjected to differential volume changes, Theor. Appl. Fract. Mech. 49 (2008) 199–205, https://doi.org/10.1016/j.tafmec.2007.11.006.
[41] H. Beushausen, M.G. Alexander, Localised strain and stress in bonded concrete overlays subjected to differential shrinkage, Mater. Struct. Constr. 40 (2007) 189–199, https://doi.org/10.1617/s11527-006-9130-z.
[42] American Society for Testing and Materials, Testing of Length Change of Hardened Concrete, ASTM C. (2016) 157–2016.
[43] K.P. Kwiatkowski, I. Stipanovic Oslakovic, H. ter Maat, A. Hartmann, P. Chinowsky, G.P.M.R. Dewulf, Modeling Cost Impacts and Adaptation of Freeze–Thaw Climate Change on a Porous Asphalt Road Network, J. Infrastruct. Syst. (2020), https://doi.org/10.1061/(asce)is.1943-555x.0000559.

[44] R. Wang, Q. Zhang, Y. Li, Deterioration of concrete under the coupling effects of freeze–thaw cycles and other actions: A review, Constr. Build. Mater. (2022), https://doi.org/10.1016/j.conbuildmat.2021.126045.
[45] A. Manawadu, P. Qiao, H. Wen, Freeze-thaw durability of shotcrete-concrete interface bonds in tension, Cold Reg. Sci. Technol. (2023), https://doi.org/10.1016/j.coldregions.2023.103798.
[46] J. Tian, X. Wu, Y. Zheng, S. Hu, W. Ren, Y. Du, et al., Investigation of damage behaviors of ECC-to-concrete interface and damage prediction model under salt freeze-thaw cycles, Constr. Build. Mater. (2019), https://doi.org/10.1016/j.conbuildmat.2019.07.237.
[47] J. Zhang, H. Li, S. Liu, L. Sun, C. Yang, R. Zhang, Effects of sulfate and freeze–thaw cycles on the bond behavior of CFRP-concrete interface, Constr. Build. Mater. (2023), https://doi.org/10.1016/j.conbuildmat.2023.130368.
[48] M. Safdar, T. Matsumoto, K. Kakuma, Flexural behavior of reinforced concrete beams repaired with ultra-high performance fiber reinforced concrete (UHPFRC, Compos Struct. (2016), https://doi.org/10.1016/j.compstruct.2016.09.010.
[49] P.A. Krahl, R. Carrazedo, M.K. El Debs, Mechanical damage evolution in UHPFRC: Experimental and numerical investigation, Eng. Struct. (2018), https://doi.org/10.1016/j.engstruct.2018.05.064.
[50] B. Graybeal, E. Brühwiler, B.-S. Kim, F. Toutlemonde, Y.L. Voo, A. Zaghi, International Perspective on UHPC in Bridge Engineering, J. Bridg Eng. 25 (2020) 04020094, https://doi.org/10.1061/(asce)be.1943-5592.0001630.
[51] T. Xie, C. Fang, M.S. Mohamad Ali, P. Visintin, Characterizations of autogenous and drying shrinkage of ultra-high performance concrete (UHPC): An experimental study, Cem. Concr. Compos 91 (2018) 156–173, https://doi.org/10.1016/j.cemconcomp.2018.05.009.
[52] Code P. Eurocode 2: design of concrete structures-part 1–1: general rules and rules for buildings. Br Stand Institution, London, 2005.
[53] D. Yoo, K. Min, J. Lee, Y. Yoon, Shrinkage and cracking of restrained ultra-high-performance fiber-reinforced concrete slabs at early age, Constr. Build. Mater. 73 (2014) 357–365, https://doi.org/10.1016/j.conbuildmat.2014.09.097.
[54] H. Huang, G. Ye, Examining the “time-zero” of autogenous shrinkage in high/ultra-high performance cement pastes, Cem. Concr. Res (2017), https://doi.org/10.1016/j.cemconres.2017.03.010.
[55] M.A. Ibrahim, M. Farhat, M.A. Issa, J.A. Hasse, Effect of material constituents on mechanical & fracture mechanics properties of ultra-high-performance concrete, Acids Struct. J. (2017), https://doi.org/10.14359/51689717.
[56] J. Wei, C. Wu, Y. Chen, C.K.Y. Leung, Shear strengthening of reinforced concrete beams with high strength strain-hardening cementitious composites (HS-SHCC), Mater. Struct. Constr. 53 (2020) 1–15, https://doi.org/10.1617/s11527-020-01537-1.
[57] GOM Correlate 2019. n.d. https://www.gom.com/en/products/zeiss-quality-suite/gom-correlate-pro.
[58] H. Herrmann, H. Bucksch, Eurocode 2 – Design of concrete structures, Dict. Geotech. Eng. Geotech. 3 (2014) 485, https://doi.org/10.1007/978-3-642-41714-6_51755.
[59] D. Gu, J. Pan, S. Mustafa, Y. Huang, M. Luković, Shear transfer mechanism in reinforced engineered cementitious composite (ECC) beams: Quantification of Vs and Vc, Eng. Struct. 261 (2022), 114282, https://doi.org/10.1016/J.ENGSTRUCT.2022.114282.
[60] A.B. Sturm, P. Visintin, D.J. Oehlers, Mechanics of shear failure in fiber-reinforced concrete beams, J. Struct. Eng. (2021), https://doi.org/10.1061/(asce)st.1943-541x.0002934.
[61] Du béton F.. Structural Connections for Precast Concrete Buildings: Guide to Good Practice. International Federation for Structural Concrete (fib); 2008.
[62] Z. Huang, Y. Tu, S. Meng, N. Bagge, J. Nilimaa, T. Blanksvärd, Validation of a numerical method for predicting shear deformation of reinforced concrete beams, Eng. Struct. (2019), https://doi.org/10.1016/j.engstruct.2019.109367.
[63] Z. Feng, C. Li, D.Y. Yoo, R. Pan, J. He, L. Ke, Flexural and cracking behaviors of reinforced UHPC beams with various reinforcement ratios and fiber contents, Eng. Struct. 248 (2021), 113266, https://doi.org/10.1016/J.ENGSTRUCT.2021.113266.
[64] H. Yin, K. Shirai, W. Teo, Numerical model for predicting the structural response of composite UHPC–concrete members considering the bond strength at the interface, Compos Struct. (2019), https://doi.org/10.1016/j.compstruct.2019.02.040.
[65] Z. Lu, Z. gang Feng, D. Yao, X. Li, H. Ji, Freeze-thaw resistance of Ultra-High performance concrete: Dependence on concrete composition, Constr. Build. Mater. (2021), https://doi.org/10.1016/j.conbuildmat.2021.123523.
[66] Z. Zhou, R. Xie, P. Qiao, L. Lu, On the modeling of tensile behavior of ultra-high performance fiber-reinforced concrete with freezing-thawing actions, Compos Part B Eng. (2019), https://doi.org/10.1016/j.compositesb.2019.106983.
[67] S. Feng, H. Xiao, R. Liu, M. Liu, The bond properties between ultra-high-performance concrete and normal strength concrete substrate: Bond macro-performance and overlay transition zone microstructure, Cem. Concr. Compos (2022), https://doi.org/10.1016/j.cemconcomp.2022.104436.
[68] K. Habel, E. Denarié, E. Brühwiler, Structural Response of Elements Combining Ultrahigh-Performance Fiber-Reinforced Concretes and Reinforced Concrete, J. Struct. Eng. (2006) https://doi.org/10.1061/(asce)0733-9445(2006)132:11(1793).
[69] a Spasojevic, D. Redaelli, M. Fernández Ruiz, A. Muttoni, Influence of tensile properties of UHPFRC on size effect in bending, Second Int Symp. Ultra High. Perform. Concr. (2008).
[70] López J.A., Serna P., Navarro-Gregori J. Advances in the development of the first UHPFRC Recommendations in Spain: Material classification, design and characterization. UHPFRC 2017 Des Build with UHPFRC New Large-Scale Implementations, Recent Tech Adv Exp Stand 2017.
[71] Červenka V., Jendele L., Červenka J. ATENA Program Documentation Part 1 Theory. Atena, 2012.
[72] A. Valikhani, A.J. Jahromi, I.M. Mantawy, A. Azizinamini, Effect of mechanical connectors on interface shear strength between concrete substrates and UHPC: Experimental and numerical studies and proposed design equation, Constr. Build. Mater. 267 (2021) 1–17, https://doi.org/10.1016/j.conbuildmat.2020.120587.
[73] A. Valikhani, A.J. Jahromi, I.M. Mantawy, A. Azizinamini, Numerical modelling of concrete-to-UHPC bond strength, Mater. (Basel) 13 (2020) 26–29, https://doi.org/10.3390/ma13061379.
[74] Q. Luo, T. Qin, Z. Chen, B. Pang, J. Qu, Z. Gao, The influence of moisture and epoxy bonding agents on interfacial behavior between normal concrete substrate and ultrahigh performance concrete as a repair material: Experimental and molecular dynamics study, Constr. Build. Mater. (2023), https://doi.org/10.1016/j.conbuildmat.2023.130779.
[75] D. Daneshvar, K. Deix, A. Robisson, Effect of casting and curing temperature on the interfacial bond strength of epoxy bonded concretes, Constr. Build. Mater. (2021), https://doi.org/10.1016/j.conbuildmat.2021.124328.
[76] J. Michels, J. Sena Cruz, R. Christen, C. Czaderski, M. Motavalli, Mechanical performance of cold-curing epoxy adhesives after different mixing and curing procedures, Compos Part B Eng. (2016), https://doi.org/10.1016/j.compositesb.2016.05.054.
[77] J. Liu, C. Vipulanandan, Tensile bonding strength of epoxy coatings to concrete substrate, Cem. Concr. Res (2005), https://doi.org/10.1016/j.cemconres.2004.06.035.
[78] A. Valikhani, A.J. Jahromi, I.M. Mantawy, A. Azizinamini, Experimental evaluation of concrete-to-UHPC bond strength with correlation to surface roughness for repair application, Constr. Build. Mater. (2020), https://doi.org/10.1016/j.conbuildmat.2019.117753.
[79] Y. Zhang, P. Zhu, Z. Liao, L. Wang, Interfacial bond properties between normal strength concrete substrate and ultra-high performance concrete as a repair material, Constr. Build. Mater. (2020), https://doi.org/10.1016/j.conbuildmat.2019.117431.
[80] M. Newlands, N. Khosravi, R. Jones, L. Chernin, Mechanical performance of statically loaded flat face epoxy bonded concrete joints, Mater. Struct. Constr. (2018), https://doi.org/10.1617/s11527-018-1175-2.
[81] D. Lau, O. Büyüköztürk, Fracture characterization of concrete/epoxy interface affected by moisture, Mech. Mater. (2010), https://doi.org/10.1016/j.mechmat.2010.09.001.
[82] Z. Wang, J.G. Dai, M. Wang, L. Chen, F. Zhang, Q. Xu, Residual bond strengths of epoxy and cement-bonded CFRP reinforcements to concrete interfaces after elevated temperature exposure, Fire Saf. J. (2021), https://doi.org/10.1016/j.firesaf.2021.103393.
[83] J. Sheng, L. chen Wang, S. ping Yin, Study on the mechanical performance of TRC-strengthened RC beams under a salt freeze–thaw environment, Cold Reg. Sci. Technol. (2021), https://doi.org/10.1016/j.coldregions.2021.103384.

[84] H. Zhao, Y. Hu, Z. Tang, K. Wang, Y. Li, W. Li, Deterioration of concrete under coupled aggressive actions associated with load, temperature and chemical attacks: A comprehensive review, Constr. Build. Mater. 322 (2022), 126466, https://doi.org/10.1016/J.CONBUILDMAT.2022.126466.
[85] ASTM C666/C666M - 03. Standard test method for resistance of concrete to rapid freezing and thawing 2008.
[86] GB/T 50082. Standard for Test Methods of Long-Term Performance and Durability of Ordinary Concrete 2009.
[87] CEN/TR 15177. Testing the freeze-thaw resistence of concrete–Internal structural damage 2006.
[88] J. Li, Z. Wu, C. Shi, Q. Yuan, Z. Zhang, Durability of ultra-high performance concrete – A review, Constr. Build. Mater. (2020), https://doi.org/10.1016/j.conbuildmat.2020.119296.